arXiv:2106.09211v2 [cs.LG] 28 Oct 2021

Square Root Principal Component Pursuit: Tuning-Free Noisy Robust Matrix Recovery

Junhui Zhang
Department of Applied Physics and Applied Math
Columbia University
New York, NY 10027
jz2903@columbia.edu

Jingkai Yan
Department of Electrical Engineering
Columbia University
New York, NY 10027
jy2927@columbia.edu

John Wright
Department of Electrical Engineering
Columbia University
New York, NY 10027
jw2966@columbia.edu

Abstract

We propose a new framework – Square Root Principal Component Pursuit – for low-rank matrix recovery from observations corrupted with noise and outliers. Inspired by the square root Lasso, this new formulation does not require prior knowledge of the noise level. We show that a single, universal choice of the regularization parameter suffices to achieve reconstruction error proportional to the (a priori unknown) noise level. In comparison, previous formulations such as stable PCP rely on noise-dependent parameters to achieve similar performance, and are therefore challenging to deploy in applications where the noise level is unknown. We validate the effectiveness of our new method through experiments on simulated and real datasets. Our simulations corroborate the claim that a universal choice of the regularization parameter yields near optimal performance across a range of noise levels, indicating that the proposed method outperforms the (somewhat loose) bound proved here.

1 Introduction

The problem of recovering a low-rank matrix from unreliable observations arises in a wide range of engineering applications, including collaborative filtering [1], latent semantic indexing [2], image and video analysis [3, 4, 5] and so on. This problem can be formalized in terms of the following observation model: given an observation $\boldsymbol{D}$ which is a superposition

$$\boldsymbol{D} = \underset{\text{low-rank}}{\boldsymbol{L}_0} + \underset{\text{sparse}}{\boldsymbol{S}_0} + \underset{\text{noise}}{\boldsymbol{Z}_0}\,. \tag{1.1}$$

35th Conference on Neural Information Processing Systems (NeurIPS 2021).

of an unknown low-rank matrix $\boldsymbol{L}_0$, sparse corruptions $\boldsymbol{S}_0$ and dense noise $\boldsymbol{Z}_0$, our goal is to accurately estimate both $\boldsymbol{L}_0$ and $\boldsymbol{S}_0$.

This model has been intensely studied, leading to algorithmic theory for methods based on both convex and nonconvex optimization [6, 7, 8]. One virtue of the convex approach is that in the noise-free setting ($\boldsymbol{Z}_0 = \boldsymbol{0}$), it is possible to exactly recover a broad range of low-rank and sparse pairs $(\boldsymbol{L}_0, \boldsymbol{S}_0)$, with a universal choice of regularization parameters, which does not depend on either the rank or sparsity. This makes it possible to deploy this method in a "hands-free" manner, provided the dataset of interest indeed has low-rank and sparse structure.

In the presence of noise, however, the situation becomes more complicated: all efficient, guaranteed estimators require knowledge of the noise level (or the rank and sparsity) [8, 9, 10]. This is problematic, since in most applications the noise level is not known ahead of time. In standard convex formulations, the appropriate regularization parameter depends on the noise standard deviation, leaving the user with a painful and time-consuming task of tuning these parameters on a per-dataset basis.

Motivated by this issue, we revisit this classical matrix recovery problem. The main contribution of this paper is the proposal and analysis of a new formulation for robust matrix recovery, which stably recovers $\boldsymbol{L}_0$ and $\boldsymbol{S}_0$ without requiring prior knowledge of the rank, sparsity, or noise level. In particular, our approach admits a single, universal choice of regularization parameters, which under standard hypotheses on $\boldsymbol{L}_0$ and $\boldsymbol{S}_0$, yields an estimation error proportional to the noise standard deviation σ. To our knowledge, our method and analysis are the first to achieve this.

Our approach is based on a combination of two natural ideas. For matrix recovery, we draw on the *stable principal component pursuit* [9], a natural convex relaxation, which minimizes a combination of the nuclear norm of $\boldsymbol{L}$, the ℓ_1 norm of $\boldsymbol{S}$ and the squared Frobenius norm $\|\boldsymbol{Z}\|_F^2$ of the noise. This is a principled approach to handling both the structured components $\boldsymbol{L}_0, \boldsymbol{S}_0$ and the noise: $\|\boldsymbol{Z}\|_F^2$ can be motivated naturally from the negative log-likelihood of the gaussian distribution. Moreover, under mild assumptions on the rank and singular vectors of $\boldsymbol{L}_0$ and the sparsity pattern of $\boldsymbol{S}_0$, the reconstruction error of stable PCP is $O(\|\boldsymbol{Z}_0\|_F)$ [9].

On the other hand, optimally balancing these terms requires knowledge of the standard deviation σ of the true noise distribution. To address this issue, we draw inspiration from the square root Lasso [11]. The square root Lasso is a sparse estimator which achieves minimax optimal estimation with a universal choice of parameters, which does not depend on the noise level. The core idea is very simple: instead of penalizing the squared Frobenius norm $\|\boldsymbol{Z}\|_F^2$ of the noise, one penalizes its square root, $\|\boldsymbol{Z}\|_F$. We call the resulting formulation *square root principal component pursuit* ($\sqrt{\text{PCP}}$). Our new formulation has the benefit that with a *noise-independent* universal choice of regularization parameters, essentially the same level of reconstruction error can be achieved. This makes $\sqrt{\text{PCP}}$ a more practical approach to low-rank recovery in unknown noise.

Due to the square root term, the objective function is no longer smooth or differentiable, and so we cannot apply algorithms such as the proximal gradient method[1]. Nevertheless, our new formulation remains convex and separable, i.e. the objective is the sum of functions of different variables, making Alternating Direction Method of Multipliers (ADMM) a suitable solver [12]. We test our new formulation with ADMM on both simulated data and real data in image processing. The experimental results show the effectiveness of our proposed new formulation in recovering the low-rank and the sparse matrix, and suggest that $\sqrt{\text{PCP}}$ has better performance than anticipated by our loose upper bound of the reconstruction error.

1.1 Notations and Assumptions

We use $\|\boldsymbol{A}\|$, $\|\boldsymbol{A}\|_F$, and $\|\boldsymbol{A}\|_*$ to denote the spectral, Frobenius, and nuclear norm of the matrix $\boldsymbol{A}$, and $\boldsymbol{A}^*$ its (conjugate) transpose. For convenience, we let $\boldsymbol{X}_0 = (\boldsymbol{L}_0, \boldsymbol{S}_0)$ be the concatenation of $\boldsymbol{L}_0$ and $\boldsymbol{S}_0$. We assume that $\boldsymbol{L}_0$ is a low-rank matrix of rank r whose compact

[1] which requires the objective to be the sum of a smooth and a non-smooth function

SVD is $\boldsymbol{L}_0 = \boldsymbol{U}\boldsymbol{\Sigma}\boldsymbol{V}^*$, $\boldsymbol{U} \in \mathbb{R}^{n_1 \times r}$, $\boldsymbol{V} \in \mathbb{R}^{n_2 \times r}$, and without loss of generality, $n_1 \geq n_2$. Let $T = \{\boldsymbol{U}\boldsymbol{Q}^* + \boldsymbol{R}\boldsymbol{V}^* | \boldsymbol{Q} \in \mathbb{R}^{n_2 \times r}, \boldsymbol{R} \in \mathbb{R}^{n_1 \times r}\}$ denote the tangent space of rank r matrices at $\boldsymbol{L}_0$. In addition, we assume that $\boldsymbol{S}_0$ is sparse with support in Ω.

Since it is impossible to disentangle $\boldsymbol{L}_0$ and $\boldsymbol{S}_0$ if the low-rank matrix $\boldsymbol{L}_0$ is sparse, or if the sparse matrix $\boldsymbol{S}_0$ is low-rank, we make the following two assumptions:

Assumption 1.1 *The low-rank matrix $\boldsymbol{L}_0$ satisfies the incoherence property with parameter ν^2, i.e.*

$$\max_i \|\boldsymbol{U}^* \boldsymbol{e}_i\|^2 \leq \frac{\nu r}{n_1}, \quad \max_i \|\boldsymbol{V}^* \boldsymbol{e}_i\|^2 \leq \frac{\nu r}{n_2}, \quad \|\boldsymbol{U}\boldsymbol{V}^*\|_\infty \leq \sqrt{\frac{\nu r}{n_1 n_2}}.$$

Assumption 1.2 *The support Ω is chosen uniformly among all sets of cardinality m, and the signs of supports are random, i.e. $P[(\boldsymbol{S}_0)_{i,j} > 0 | (i,j) \in \Omega] = P[(\boldsymbol{S}_0)_{i,j} < 0 | (i,j) \in \Omega] = 0.5$.*

These assumptions follow [6]; indeed, our proof makes use of a dual certificate constructed for noiseless low-rank and sparse recovery in that paper.

1.2 Problem Formulation and Main Results

Inspired by square root Lasso, we propose to solve the robust noisy matrix recovery problem through the following optimization problem:

$$\sqrt{\text{PCP}} \ : \min_{\boldsymbol{L},\boldsymbol{S}} \ \|\boldsymbol{L}\|_* + \lambda \|\boldsymbol{S}\|_1 + \mu \|\boldsymbol{L} + \boldsymbol{S} - \boldsymbol{D}\|_F \,. \tag{1.2}$$

The parameter λ that balances the low-rank and the sparse regularizers is studied in [6], where it is shown that $\lambda = 1/\sqrt{n_1}$ gives exact recovery when $\boldsymbol{Z}_0 = \boldsymbol{0}$ and the $\mu \|\boldsymbol{L} + \boldsymbol{S} - \boldsymbol{D}\|_F$ penalty term in (1.2) is replaced with the constraint $\boldsymbol{L} + \boldsymbol{S} = \boldsymbol{D}$. In this work, we build on this result and focus on the parameter μ. Our main result is that under the aforementioned (standard) hypotheses on $\boldsymbol{L}_0$ and $\boldsymbol{S}_0$, using a single, universal choice $\mu = \sqrt{n_2/2}$, $\sqrt{\text{PCP}}$ recovers $\boldsymbol{L}_0$ and $\boldsymbol{S}_0$, with an estimation error that is proportional to the norm of the noise:

Theorem 1.1 *Under Assumptions 1.1 and 1.2, provided that r, m satisfies*

$$r \leq \rho_r n_2 \nu^{-1} (\log n_1)^{-2}, \quad m \leq \rho_s n_1 n_2, \tag{1.3}$$

where $\rho_r \leq 1/10$, ρ_s are some positive constants. Then there is a numerical constant c such that with probability at least $1 - c n_1^{-10}$, the $\sqrt{PCP}$ problem (1.2) with $\lambda = 1/\sqrt{n_1}$ and $\mu = \sqrt{n_2/2}$ produces a solution $\widehat{\boldsymbol{X}} = (\widehat{\boldsymbol{L}}, \widehat{\boldsymbol{S}})$ such that

$$\|\widehat{\boldsymbol{X}} - \boldsymbol{X}_0\|_F \leq 560 \sqrt{n_1 n_2} \|\boldsymbol{Z}_0\|_F. \tag{1.4}$$

Why is it possible to achieve accurate estimation with a single choice of μ? We draw intuition from a connection to the *stable principal component pursuit* formulations studied in [9]. This work studies both constrained and unconstrained formulations:

$$\text{StablePCP}_c : \min_{\boldsymbol{L},\boldsymbol{S}} \ \|\boldsymbol{L}\|_* + \lambda \|\boldsymbol{S}\|_1 \ s.t. \ \|\boldsymbol{L} + \boldsymbol{S} - \boldsymbol{D}\|_F \leq \delta. \tag{1.5}$$

$$\text{StablePCP}_u : \min_{\boldsymbol{L},\boldsymbol{S}} \ \|\boldsymbol{L}\|_* + \lambda \|\boldsymbol{S}\|_1 + \frac{\bar{\mu}}{2} \|\boldsymbol{L} + \boldsymbol{S} - \boldsymbol{D}\|_F^2. \tag{1.6}$$

These formulations are equivalent, and equivalent to $\sqrt{\text{PCP}}$ in the following sense: for each problem instance, there is a calibration of parameters $\delta \leftrightarrow \bar{\mu} \leftrightarrow \mu$ such that $\sqrt{\text{PCP}}$, StablePCP_u and StablePCP_c have exactly the same set of optimal solutions. However, (1.5)-(1.6) require that the parameters δ and $\bar{\mu}$ be determined on an instance-by-instance basis, based on the noise level. Choosing these parameters correctly is essential: in (1.5), δ should be chosen to be larger than $\|\boldsymbol{Z}_0\|_F$. For square ($n_1 = n_2 = n$) matrices, in a stochastic setting in which $(\boldsymbol{Z}_0)_{ij}$ are iid $\mathcal{N}(0, \sigma^2)$, following [9], $\bar{\mu}$ can be chosen as $\frac{1}{2\sigma\sqrt{n}}$. This follows from

[2] $\nu \geq 1$ since $\|\boldsymbol{U}\|_F^2 = r$, and so $\max_i \|\boldsymbol{U}^* \boldsymbol{e}_i\|^2 \geq \frac{r}{n_1}$.

the fact that in this setting $n^{-1/2}\|\boldsymbol{Z}_0\| \to 2\sigma$ almost surely; setting $\bar{\mu}$ in this fashion ensures that the singular value shrinkage induced by the nuclear norm regularizer $\|\cdot\|_*$ is greater than the largest singular value of $\boldsymbol{Z}_0$.

In contrast to this σ-dependent penalty parameter, fixing $\boldsymbol{S} = \boldsymbol{S}_0$, $\sqrt{\text{PCP}}$ formulation (1.2) requires that $\mathbf{0} \in \partial(\|\widehat{\boldsymbol{L}}\|_* + \mu\|\widehat{\boldsymbol{L}} - \boldsymbol{Z}_0 - \boldsymbol{L}_0\|_F)$, which translates into $-\mu\frac{\widehat{\boldsymbol{L}}-\boldsymbol{Z}_0-\boldsymbol{L}_0}{\|\widehat{\boldsymbol{L}}-\boldsymbol{Z}_0-\boldsymbol{L}_0\|_F} \in \partial\|\widehat{\boldsymbol{L}}\|_*$. With the hope that $\widehat{\boldsymbol{L}} \approx \boldsymbol{L}_0$, and by the subdifferential formulation[3], we have $\mu\frac{\|\boldsymbol{Z}_0\|}{\|\boldsymbol{Z}_0\|_F} \approx 1$. The concentration stated above then gives an intuitive choice for $\mu \approx \frac{n\sigma}{2\sigma\sqrt{n}}$, or $\mu = c_0\sqrt{n}$ for some $c_0 > 0$. The magic of $\sqrt{\text{PCP}}$ is that by using the Frobenius norm instead of its square, the objective function becomes homogeneous, i.e. the gradient of the penalty term at the ground truth $\boldsymbol{X}_0$ becomes σ independent, making a universal penalty parameter possible.

1.3 Relationship to the Literature

The problem of low-rank matrix recovery from gross sparse corruption can be considered a form of robust PCA, [6, 13], and has been studied extensively in the literature. Algorithmic theory has been developed for both convex [6, 13, 14, 15, 16], and nonconvex optimization methods [7, 8, 17, 18, 19]. While many of the aforementioned works pertain to noiseless data, a line of work has studied extensions to noisy data. [9] studied the problem of robust matrix recovery with bounded noise under the incoherence assumption, and proved a bound on the recovery error, with linear dependence on the noise level but suboptimal dependence on the matrix size. [20] studied the problem with a weaker assumption about spikiness using decomposable regularizers and restricted strong convexity (RSC), and obtained essentially optimal bounds on the reconstruction error when the noise level is large. These weaker assumptions are not sufficient to ensure exact recovery, and so when the noise standard deviation σ is small, this approach does not yield a reconstruction error proportional to the noise level. [10] formulated robust PCA as a semidefinite programming problem, which requires strong assumptions about square matrices and positive semidefiniteness of the low-rank matrix. Some other works [21, 22] further assumed partial observation of the matrix, and also derived tighter bounds on the recovery error. The recent work of [8] achieves optimal error bounds for both large and small noise, using a novel analysis that leverages an auxiliary nonconvex program. Taken together, these results give efficient and provably effective methods, whose statistical performance is nearly optimal. Compared to e.g., [8, 20], the stability guarantees provided by our theory are worse by a dimension-dependent factor. Nevertheless, all of the above works regarding robust PCA with noise, the optimization involves parameters that must be set based on the noise level distribution, and therefore challenging in actual applications.

On the other hand, there has been existing work in the literature on structured signal recovery without needing to know the noise level. Our proposed square root PCP is directly inspired by the square root Lasso [11], which proposed the idea of replacing the squared loss with its "square root" version. This allows for a choice of the parameter independent of noise level, while maintaining near-oracle performance. Later works have extended this idea to other scenarios, such as group lasso [23], SLOPE variable selection [24], elastic net [25] and matrix completion [26], etc. Notably, the work of [26] studied the matrix completion where one aims to recover a low-rank matrix from noisy linear observations, aka matrix completion. Compared with that paper, this work aims to solve a different problem where the observation also contains a sparse outlier matrix. To the best of our knowledge, this paper is the first to propose a provable algorithm for Robust PCA with noisy observation that does not require knowledge of the noise level beforehand. On the algorithmic side, interior point method and first order method are used to solve the square root Lasso in [11], while later works apply ADMM to the problem [27][28]. In our problem, the objective function can be transformed into a separable form, making ADMM a reasonable choice.

We note that for large σ the error bound established in this paper is suboptimal compared with [11] and [26]. The problem of square root lasso enjoys benign properties (lower bounds on restricted eigenvalues) which we do not have in square root PCP. The paper [26] on matrix completion makes a spikiness assumption, and proves that a square root

[3]The subdifferential of a norm satisfies $\partial\|x\| = \{z \mid \langle x, z\rangle = \|x\|, \|z\|^* \le 1\}$.

lasso-inspired formulation achieves essentially optimal estimation when the noise is large. As with robust matrix recovery, the spikiness assumption is not strong enough to imply exact recovery in the noiseless case. Compared to these works, the principal differences in this paper are (i) the problem formulation: we consider robust PCA with sparse errors, (ii) the analysis, which proceeds down different lines, and (iii) that our bounds are linear in the noise level, for both large and small noise. However, in contrast to [26], our analysis does not yield minimax optimal estimation errors; it is worse by a dimension-dependent factor. Improving this dependence is an important direction for future work.

2 Analysis

The proof of the main Theorem 1.1 is different from the standard approach in [11] due to a lack of the Restricted Strong Convexity property for the map $(\boldsymbol{L}, \boldsymbol{S}) \to \|\boldsymbol{L} + \boldsymbol{S} - \boldsymbol{D}\|_F$. Instead, our approach has three key ingredients:

- The result from StablePCP$_c$ (Theorem 2.1) shows a recovery error $\|(\widehat{\boldsymbol{L}}, \widehat{\boldsymbol{S}}) - (\boldsymbol{L}_0, \boldsymbol{S}_0)\|_F$ which depends linearly on the parameter δ.
- The intimate connection between $\sqrt{\text{PCP}}$ formulation (1.2) and StablePCP$_c$ formulation (1.5) can help translate the above solution property to $\sqrt{\text{PCP}}$ (Lemma 2.2).
- The powerful dual certificate construction proposed in [6] (restated in Lemma 2.3) can be used as an approximate subgradient to bound the regularizer at $\widehat{\boldsymbol{X}}$.

The proof of the main theorem has two steps. First, it uses the optimality condition and the subgradient to provide an upper and an lower bound for the regularization terms at $\widehat{\boldsymbol{X}}$. Second, the result in Theorem 2.1 is translated into the $\sqrt{\text{PCP}}$ setting, and together with the bounds obtained above, we get the desired result. The proof is given in the supplementary material, and below we provide three ingredients.

First, we state the main theorem for StablePCP$_c$ problem:

Theorem 2.1 (Theorem 2 in [9]) *Under Assumptions 1.1 and 1.2, assuming further that $r \leq \rho_r' n_2 \nu^{-1} (\log n_1)^{-2}$ and $m \leq \rho_s' n_1 n_2$ where ρ_r', ρ_s' are some positive constants, there is a numerical constant c' such that with probability at least $1 - c' n_1^{-10}$, for any $\boldsymbol{Z}_0$ with $\|\boldsymbol{Z}_0\|_F \leq \delta$, the solution $\widehat{\boldsymbol{X}} = (\widehat{\boldsymbol{L}}, \widehat{\boldsymbol{S}})$ to the StablePCP$_c$ problem 1.5 with $\lambda = 1/\sqrt{n_1}$ satisfies*

$$\|\widehat{\boldsymbol{X}} - \boldsymbol{X}_0\|_F \leq \sqrt{320 n_1 n_2 + 4} \cdot \delta. \tag{2.1}$$

Note that choosing $\delta = \|\boldsymbol{Z}_0\|_F$ allows a reconstruction error that is $O(\sqrt{n_1 n_2}\|\boldsymbol{Z}_0\|_F)$. In the case when $\boldsymbol{Z}_0 = \boldsymbol{0}$, StablePCP$_c$ recovers the matrices exactly: $\widehat{\boldsymbol{X}} = \boldsymbol{X}_0$. This is in agreement with the result in [6]. The next lemma connects the two formulations $\sqrt{\text{PCP}}$ and StablePCP$_c$ and the proof is provided in the supplementary material:

Lemma 2.2 *Consider the $\sqrt{PCP}$ problem parameterized by μ and denote the result as $\widehat{\boldsymbol{L}}_{\text{root}}(\mu), \widehat{\boldsymbol{S}}_{\text{root}}(\mu)$, as well as the StablePCP$_c$ formulation parameterized by δ and denote the result as $\widehat{\boldsymbol{L}}_{\text{stable}}(\delta), \widehat{\boldsymbol{S}}_{\text{stable}}(\delta)$. Define $\delta(\mu) = \|\boldsymbol{D} - \widehat{\boldsymbol{L}}_{\text{root}}(\mu) - \widehat{\boldsymbol{S}}_{\text{root}}(\mu)\|_F$, then*

$$\widehat{\boldsymbol{L}}_{\text{stable}}(\delta(\mu)), \widehat{\boldsymbol{S}}_{\text{stable}}(\delta(\mu)) = \widehat{\boldsymbol{L}}_{\text{root}}(\mu), \widehat{\boldsymbol{S}}_{\text{root}}(\mu). \tag{2.2}$$

Lastly, we show an adapted dual certificate construction:

Lemma 2.3 (Adapted from [6]) *Under Assumptions 1.1 and 1.2, assume that r, m satisfies*

$$r \leq \rho_r n_2 \nu^{-1} (\log n_1)^{-2}, \quad m \leq \rho_s n_1 n_2, \tag{2.3}$$

where $\rho_r \leq 1/10, \rho_s$ are some positive constants. Then there is a numerical constant c such that with probability at least $1 - c n_1^{-10}$, there exists $\boldsymbol{W}, \boldsymbol{F}, \boldsymbol{H}$ such that

$$\boldsymbol{U}\boldsymbol{V}^* + \boldsymbol{W} = \lambda(\text{sign}(\boldsymbol{S}_0) + \boldsymbol{F} + P_\Omega \boldsymbol{H}), \tag{2.4}$$

where $\boldsymbol{W} \in T^\perp$, $\|\boldsymbol{W}\| \leq \frac{1}{2}$, $P_\Omega \boldsymbol{F} = \boldsymbol{0}$, $\|\boldsymbol{F}\|_\infty \leq \frac{1}{2}$, and $\|P_\Omega \boldsymbol{H}\|_F \leq \frac{1}{260\sqrt{2}}$.

The dual construction in [6] satisfies $\|P_\Omega \boldsymbol{H}\|_F \le \frac{1}{4}$. However, the proof for Lemma 2.8(b) indicates that $\|P_\Omega \boldsymbol{H}\|_F \le \frac{\sqrt{r}}{n_1^2} \le \frac{\sqrt{r/n_2}}{n_1^{1.5}}$ and we only need to make sure that $\frac{\sqrt{r/n_2}}{n_1^{1.5}} \le \frac{1}{260\sqrt{2}}$. This is a very mild condition, especially when it comes to the high dimensional real data (such as video). If we require that $r \le n_2/10$, then problems of reasonably large dimension suffice, say, $n_1 \ge 120$. And in the extreme case, we can set $\rho_r \le 1/(260\sqrt{2})^2$.

3 Solving $\sqrt{\text{PCP}}$ with ADMM

Different from [9] where StablePCP$_u$ (1.6) is solved via *Accelerated Proximal Gradient* method, we solve $\sqrt{\text{PCP}}$ (and StablePCP$_u$) via ADMM-splitting since the objective is not differentiable. To avoid multi-block ADMM which is not guaranteed to converge [29], we define variables $\boldsymbol{X}_1^* = (\boldsymbol{L}_1^*, \boldsymbol{S}_1^*, \boldsymbol{Z}^*),\ \boldsymbol{X}_2^* = (\boldsymbol{L}_2^*, \boldsymbol{S}_2^*)$, and reformulate problem (1.2) as:

$$\begin{aligned} \min_{\boldsymbol{X}_1, \boldsymbol{X}_2}\ & f(\boldsymbol{X}_1) := \|\boldsymbol{L}_1\|_* + \lambda\|\boldsymbol{S}_1\|_1 + \mu\|\boldsymbol{Z}\|_F \\ \text{s.t.}\quad & \boldsymbol{X}_1 + \begin{bmatrix} -\boldsymbol{I} & \boldsymbol{0} \\ \boldsymbol{0} & -\boldsymbol{I} \\ \boldsymbol{I} & \boldsymbol{I} \end{bmatrix} \boldsymbol{X}_2 = \begin{bmatrix} \boldsymbol{0} \\ \boldsymbol{0} \\ \boldsymbol{D} \end{bmatrix}. \end{aligned} \tag{3.1}$$

The problem (3.1) can be separated into 2 blocks nicely ($\boldsymbol{X}_1$ and $\boldsymbol{X}_2$), which guarantees convergence of ADMM (under additional mild conditions)[12].

Define dual variables $\boldsymbol{Y}^* = (\boldsymbol{Y}_1^*, \boldsymbol{Y}_2^*, \boldsymbol{Y}_3^*)$, the Lagrangian can be written as

$$\begin{aligned} \mathcal{L}_\rho(\boldsymbol{X}_1, \boldsymbol{X}_2, \boldsymbol{Y}) = \|\boldsymbol{L}_1\|_* + \lambda\|\boldsymbol{S}_1\|_1 + \mu\|\boldsymbol{Z}\|_F + \langle \boldsymbol{L}_1 - \boldsymbol{L}_2, \boldsymbol{Y}_1\rangle + \frac{\rho}{2}\|\boldsymbol{L}_1 - \boldsymbol{L}_2\|_F^2 + \langle \boldsymbol{S}_1 - \boldsymbol{S}_2, \boldsymbol{Y}_2\rangle \\ + \frac{\rho}{2}\|\boldsymbol{S}_1 - \boldsymbol{S}_2\|_F^2 + \langle \boldsymbol{L}_2 + \boldsymbol{S}_2 + \boldsymbol{Z} - \boldsymbol{D}, \boldsymbol{Y}_3\rangle + \frac{\rho}{2}\|\boldsymbol{L}_2 + \boldsymbol{S}_2 + \boldsymbol{Z} - \boldsymbol{D}\|_F^2. \end{aligned}$$

We present the update rules[4] as well as the stopping criteria adapted from [12] in Algorithm 1 and `helper()` function in the supplementary material. The stopping criteria takes into account the primal and the dual feasibility conditions, and the algorithm stops when the tolerances set using an absolute and relative criterion are reached.

If we modify the update of $\boldsymbol{Z}$ in Algorithm 1 to $\boldsymbol{Z} \leftarrow \left(\boldsymbol{D} - \boldsymbol{L}_2 - \boldsymbol{S}_2 - \frac{1}{\rho}\boldsymbol{Y}_3\right)/(1 + \mu/\rho)$, we get ADMM for StablePCP$_u$ (1.6).

Algorithm 1 Algorithm for $\sqrt{\text{PCP}}$

Input: $\boldsymbol{D} \in \mathbb{R}^{n_1 \times n_2}, \lambda, \mu$.
Output: $\boldsymbol{L}, \boldsymbol{S} \in \mathbb{R}^{n_1 \times n_2}$.

 # Tolerance levels, max iterations
$\epsilon_{\text{abs}} \leftarrow 10^{-6}, \epsilon_{\text{rel}} \leftarrow 10^{-6}, N \leftarrow 5000$
 # Initialization
$\boldsymbol{L}_1, \boldsymbol{L}_2, \boldsymbol{S}_1, \boldsymbol{S}_2, \boldsymbol{Z}, \boldsymbol{Y}_1, \boldsymbol{Y}_2, \boldsymbol{Y}_3 \leftarrow \boldsymbol{0}_{n_1 \times n_2}$
$\rho \leftarrow 0.1$
for $i = 1, i \le N, i{+}{+}$ **do**
  # Save old values temporarily
  $(\boldsymbol{L}_2', \boldsymbol{S}_2') \leftarrow (\boldsymbol{L}_2, \boldsymbol{S}_2)$
  # ADMM updates
  $\boldsymbol{L}_1 \leftarrow \text{prox}_{\frac{1}{\rho}\|\cdot\|_*}\left(\boldsymbol{L}_2 - \frac{1}{\rho}\boldsymbol{Y}_1\right)$
  $\boldsymbol{S}_1 \leftarrow \text{prox}_{\frac{\lambda}{\rho}\|\cdot\|_1}\left(\boldsymbol{S}_2 - \frac{1}{\rho}\boldsymbol{Y}_2\right)$
  $\boldsymbol{Z} \leftarrow \text{prox}_{\frac{\mu}{\rho}\|\cdot\|_F}\left(\boldsymbol{D} - \boldsymbol{L}_2 - \boldsymbol{S}_2 - \frac{1}{\rho}\boldsymbol{Y}_3\right)$
  $\boldsymbol{L}_2 \leftarrow \frac{\left(\boldsymbol{D} - \boldsymbol{Z} + 2\boldsymbol{L}_1 - \boldsymbol{S}_1 + \frac{1}{\rho}(2\boldsymbol{Y}_1 - \boldsymbol{Y}_2 - \boldsymbol{Y}_3)\right)}{3}$
  $\boldsymbol{S}_2 \leftarrow \frac{\left(\boldsymbol{D} - \boldsymbol{Z} + 2\boldsymbol{S}_1 - \boldsymbol{L}_1 + \frac{1}{\rho}(2\boldsymbol{Y}_2 - \boldsymbol{Y}_1 - \boldsymbol{Y}_3)\right)}{3}$
  $\boldsymbol{Y}_1 \leftarrow \boldsymbol{Y}_1 + \rho(\boldsymbol{L}_1 - \boldsymbol{L}_2)$
  $\boldsymbol{Y}_2 \leftarrow \boldsymbol{Y}_2 + \rho(\boldsymbol{S}_1 - \boldsymbol{S}_2)$
  $\boldsymbol{Y}_3 \leftarrow \boldsymbol{Y}_3 + \rho(\boldsymbol{L}_2 + \boldsymbol{S}_2 + \boldsymbol{Z} - \boldsymbol{D})$
  # Update ρ and check convergence
  ρ, ifConverge $\leftarrow$ `helper()`
  if ifConverge **then**
    break
  end if
end for
$(\boldsymbol{L}, \boldsymbol{S}) \leftarrow ((\boldsymbol{L}_1 + \boldsymbol{L}_2)/2, (\boldsymbol{S}_1 + \boldsymbol{S}_2)/2)$
return $\boldsymbol{L}, \boldsymbol{S}$

[4] Recall that $\text{prox}_{\gamma\|\cdot\|_*}(\boldsymbol{Z}) = \sum_i \max(\lambda_i - \gamma, 0)\boldsymbol{u}_i\boldsymbol{v}_i^*$, where $\boldsymbol{Z} = \sum_i \lambda_i \boldsymbol{u}_i \boldsymbol{v}_i^*$ is the SVD, $[\text{prox}_{\gamma\|\cdot\|_1}(\boldsymbol{Z})]_{i,j} = \max(|\boldsymbol{Z}_{i,j}| - \gamma, 0) \cdot \text{sign}(\boldsymbol{Z}_{i,j})$, and $\text{prox}_{\gamma\|\cdot\|_F}(\boldsymbol{Z}) = \max(\|\boldsymbol{Z}\|_F - \gamma, 0)\frac{\boldsymbol{Z}}{\|\boldsymbol{Z}\|_F}$.

4 Experiments

To show the effectiveness of our new formulation, we test $\sqrt{\text{PCP}}$ on simulated data as well as real-world video datasets. The experiments suggest that our error bound in Theorem 1.1 has a correct dependency on the noise level of $\boldsymbol{Z}_0$, but loses a factor of n (the dimension of the problem). In addition, the solutions produced by $\sqrt{\text{PCP}}$ with our proposed noise-independent μ and StablePCP$_u$ with the noise-dependent μ often look very similar to each other. Moreover, experiments on real-world datasets with natural noise also show the denoising effect of $\sqrt{\text{PCP}}$, making $\sqrt{\text{PCP}}$ a practical approach with good performance in this robust noisy low-rank matrix recovery setting.

Additional experiments of $\sqrt{\text{PCP}}$ on simulated data with varying μ also suggest that $\sqrt{n_2/2}$ can provide performance (recovery error) close to the optimal μ, justifying our proposed choice of $\mu = \sqrt{n_2/2}$.

4.1 Simulations with Varying Noise Levels and Dimension

In this set of experiments, we are interested in how our error bound in Theorem 1.1 compare with the actual reconstruction error. We simulate $(\boldsymbol{L}_0, \boldsymbol{S}_0, \boldsymbol{Z}_0)$ with varying noise levels of $\boldsymbol{Z}_0$ and problem dimension n_1, n_2. To simulate $\boldsymbol{L}_0 \in \mathbb{R}^{n_1 \times n_2}$ of rank r, we generate $\boldsymbol{U} \in \mathbb{R}^{n_1 \times r}, \boldsymbol{V} \in \mathbb{R}^{n_2 \times r}$ as the unnormalized singular vectors such that $\boldsymbol{U}, \boldsymbol{V}$ are entrywise i.i.d. $\mathcal{N}(0, 1/n_1)$ and $\mathcal{N}(0, 1/n_2)$ respectively and let $\boldsymbol{L}_0 = \boldsymbol{U}\boldsymbol{V}^*$. For $\boldsymbol{S}_0$, we let $P[(i,j) \in \Omega] = \rho_S$ and for (i,j) in support Ω, $(\boldsymbol{S}_0)_{(i,j)} \in \{0.05, -0.05\}$ with equal probability. For the noise $\boldsymbol{Z}_0$, we generate it as entrywise i.i.d. $\mathcal{N}(0, \sigma^2)$.

In addition, in the experiments we take $n_1 = n_2 = n$, so we choose $\lambda = 1/\sqrt{n}$, $\mu_{\text{stable}} = 1/(2\sigma\sqrt{n})$ (the noise level σ is known), and $\mu_{\text{root}} = \sqrt{n/2}$. Theoretical analysis in Theorem 1.1 and 2.1 shows that with these parameters, $\|\widehat{\boldsymbol{X}} - \boldsymbol{X}_0\|_F = O(n\|\boldsymbol{Z}_0\|_F)$.

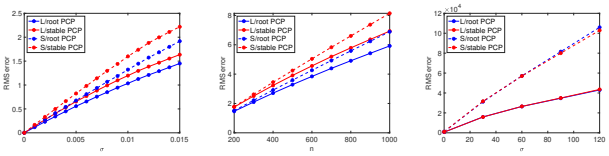
To test the dependency of the error on σ, we take $n = 200$, $r = 10$, and so $\|\boldsymbol{L}_0\|_F^2 \approx r = 10$. For the outlier $\boldsymbol{S}_0$, we take $\rho_S = 0.1$, so $\|\boldsymbol{S}_0\|_F^2 \approx 0.05^2 n^2 \rho_S = 10$. For the noise $\boldsymbol{Z}_0$, we take $\sigma \in \{0, 0.001, \ldots, 0.015\}$[5], so $\|\boldsymbol{Z}_0\|_F^2 \approx \sigma^2 n^2 \in [0, 9]$. For each σ in the given set, we randomly generate 20 ground truth $(\boldsymbol{L}_0, \boldsymbol{S}_0, \boldsymbol{Z}_0)$ triplets and run $\sqrt{\text{PCP}}$ and StablePCP$_u$ on them. We use the root-mean-squared (RMS) error defined as $(\frac{1}{20}\sum_{k=1}^{20} \|\widehat{\boldsymbol{L}}^{(k)} - \boldsymbol{L}_0\|_F^2)^{1/2}$ and $(\frac{1}{20}\sum_{k=1}^{20} \|\widehat{\boldsymbol{S}}^{(k)} - \boldsymbol{S}_0\|_F^2)^{1/2}$ for evaluation. In Figure 1(a) we show the RMS error over 20 trials for the low-rank and the sparse. It is clear from the plot that $\|\widehat{\boldsymbol{L}} - \boldsymbol{L}_0\|_F$ and $\|\widehat{\boldsymbol{S}} - \boldsymbol{S}_0\|_F$ are $O(\sigma)$ for both $\sqrt{\text{PCP}}$ and StablePCP$_u$, which confirms that the reconstruction error is linear in the noise level σ.

We also notice that the recovery error in Figures 1(a) and 1(c) is linear in the noise level for small σ, but exhibits a sublinear behavior for larger σ. This behavior reflects a general phenomenon in recovery/denoising using structured models (sparse, low-rank, etc.): the minimax noise sensitivity $\eta = \sup_{\sigma>0} \frac{1}{\sigma} E[\|\widehat{\boldsymbol{x}} - \boldsymbol{x}_0\|]$ is obtained as $\sigma \to 0$. This means that for small σ, we expect a linear trend with slope η, while for larger σ, the dependence can be sublinear. This behavior has a general geometric explanation. For simplicity we sketch how this plays out in a simpler norm denoising problem, in which the target is to recover a structured signal $\boldsymbol{x}_0$, and we observe $\boldsymbol{y} = \boldsymbol{x}_0 + \sigma\boldsymbol{z}$. For simplicity, assume that we know that $\|\boldsymbol{x}_0\|_1 \le \tau$, and solve $\min_{\|\boldsymbol{x}\|_1 \le \tau} \|\boldsymbol{x} - \boldsymbol{y}\|_2$. For small σ, the estimation error $\widehat{\boldsymbol{x}} - \boldsymbol{x}_0$ is simply the projection of the noise $\sigma\boldsymbol{z}$ onto the descent cone of the norm ball $\{\|\boldsymbol{x}\|_1 \le \tau\}$ at $\boldsymbol{x}_0$; its size is linear in σ. For larger σ, there is additional denoising due to the fact that the L1 ball is smaller than the descent cone at $\boldsymbol{x}_0$ — this leads to the behavior observed here.

To test the dependency of the error on the problem dimension, we vary $n \in \{200, 300, \ldots, 1000\}$ and take $r = 0.1n$. We keep the setting for $\boldsymbol{S}_0$, and take $\sigma = 0.01$ as the noise level for $\boldsymbol{Z}_0$. Figure 1(b) shows the RMS error. Note that for fixed σ, $\|\boldsymbol{Z}_0\|_F \sim n\sigma$, so the results in Theorem 1.1 and Theorem 2.1 bound the reconstruction error as $O(n^2)$.

[5]When $\sigma = 0$ and $\mu_{\text{stable}} = +\infty$, StablePCP$_u$ is equivalent to StablePCP$_c$ with $\delta = 0$.

However, the analysis provides only a loose error bound. As can be seen from this set of experiment, the error is closer to $O(n)$. We provide experiments with different distributions of the noise in the appendix.



(a) RMSE, vary σ (b) RMSE, vary n (c) "hall" + noise

Figure 1: StablePCP$_u$ vs $\sqrt{\text{PCP}}$: a,b): simulated, c): hall

4.2 Real Data with Added Noise: Surveillance Video

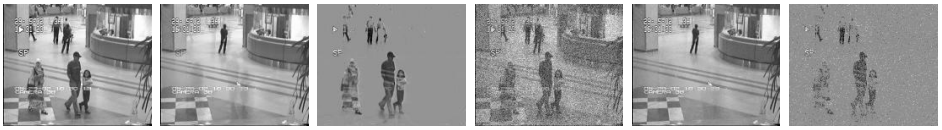
Many imaging datasets can be modeled as the sum of a low-rank matrix $\boldsymbol{L}_0$, a sparse outlier $\boldsymbol{S}_0$, and noise $\boldsymbol{Z}_0$. For instance, video data often consists of an almost fixed background which can be seen as low-rank, and a foreground (such as people) that only occupies a small fraction of the image pixels for a short amount of time, which can be considered as sparse. Thus, videos can naturally fit into our robust PCA framework.

In this set of experiments, we use $\sqrt{\text{PCP}}$ and StablePCP$_u$ to separate the background and the foreground for surveillance video data. We assume that the original video is noiseless, and manually add noise $\boldsymbol{Z}_0$ that is entrywise i.i.d. $\mathcal{N}(0, \sigma^2)$ to test the dependency of the reconstruction error on the noise level σ.

We use the "hall dataset" in [30], a 200-frame video of a hall that has people walking around. Each frame has resolution 144×176, and is flattened as one column of the noiseless observation matrix $\boldsymbol{D}$, so we have $n_1 = 144 \times 176$ and $n_2 = 200$. Each pixel is represented by a number in $[0, 255]$, and the mean value among all pixels is 150.3295, with standard deviation 45.7438, and median 155.0000.

For the added noise, we choose $\sigma \in \{0, 30, 60, 90, 120\}$, and denote the recovered matrices as $\widehat{\boldsymbol{X}}^{(\sigma)}_{\text{root/stable}}$. In addition, we let $\boldsymbol{X}_0 = \frac{1}{2}(\widehat{\boldsymbol{X}}^{(0)}_{\text{root}} + \widehat{\boldsymbol{X}}^{(0)}_{\text{stable}})$ be the ground truth, and evaluate the error using $\|\widehat{\boldsymbol{L}}^{(\sigma)}_{\text{root/stable}} - \boldsymbol{L}_0\|_F$ and $\|\widehat{\boldsymbol{S}}^{(\sigma)}_{\text{root/stable}} - \boldsymbol{S}_0\|_F$. We take $\lambda = 1/\sqrt{n_1}$, $\mu_{\text{root}} = \sqrt{n_2/2}$ and $\mu_{\text{stable}} = \frac{1}{\sigma(\sqrt{n_1}+\sqrt{n_2})}$ following the same intuition as in Section 1.[6] We run the experiments on a laptop with 2.3 GHz Dual-Core Intel Core i5, and set the maximal iteration of ADMM to be 5000. All of these experiments on real datasets end within 1 hour. For full details, please see the supplementary material.

In Figure 1(c), we show the reconstruction error with varying noise levels. It can be seen that the error is indeed linear in σ, as predicted by our analysis. In Figures 2, we present the first frame (i.e. the first column) of the original video (with noise $\sigma = 0, 30$), and the $\sqrt{\text{PCP}}$ recovered low-rank and sparse matrices. Although the added noise blurs the videos, our $\sqrt{\text{PCP}}$ is still stable and successfully decompose the background and the foreground.



(a) video (b) $\widehat{\boldsymbol{L}}^{(0)}_{\text{root}}$ (c) $\widehat{\boldsymbol{S}}^{(0)}_{\text{root}}$ (d) video+$\boldsymbol{Z}_0$ (e) $\widehat{\boldsymbol{L}}^{(30)}_{\text{root}}$ (f) $\widehat{\boldsymbol{S}}^{(30)}_{\text{root}}$

Figure 2: hall frame 1: $\sqrt{\text{PCP}}$ for $\sigma = 0, 30$

4.3 Real Data with Natural Noise: Low Light Video

Low light videos are known to have very large observation noise due to limited photon counts. In this experiment, we apply our $\sqrt{\text{PCP}}$ to the Dark Raw Video (DRV) dataset in [32] (under MIT License) for foreground background separation and denoising. This dataset of

[6] Recall that $E[\|\boldsymbol{Z}_0\|] \leq \sigma(\sqrt{n_1} + \sqrt{n_2})$ for rectangular matrices, e.g. from [31]

RGB videos, approximately 110 frames each, 3672×5496 in resolution, was collected at low light settings, so the signal-to-noise ratio (SNR) is extremely low (negative if measured in dB)[32].

For the experiments, we choose video M0001 (basketball player), M0004 (toy windmill), and M0009 (billiard table) from DRV. As preprocessing, we convert the RGB videos to grayscale using `rgb2gray()` in Matlab, and crop and downsample each frame to reduce data size. The final resolution is 322×440 for M0001, 294×440 for M0004, and 306×458 for M0009.

We apply $\sqrt{\text{PCP}}$ with $\lambda = 1/\sqrt{n_1}$, and $\mu = \sqrt{n_2/2}$ to these 3 videos, and present the results for frame 30 in Figure 3. The denoising effect of $\sqrt{\text{PCP}}$ can be seen by comparing $\boldsymbol{D}$ with $\widehat{\boldsymbol{L}}+\widehat{\boldsymbol{S}}$. In addition, $\widehat{\boldsymbol{L}}$ recovers the background pretty well, $\widehat{\boldsymbol{S}}$ captures the moving foreground but is still mixed with noise, which we believe is due to the extremely low SNR.

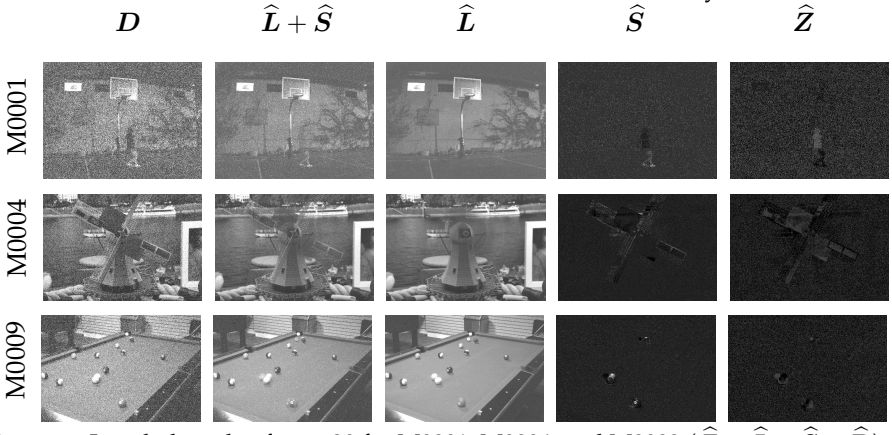
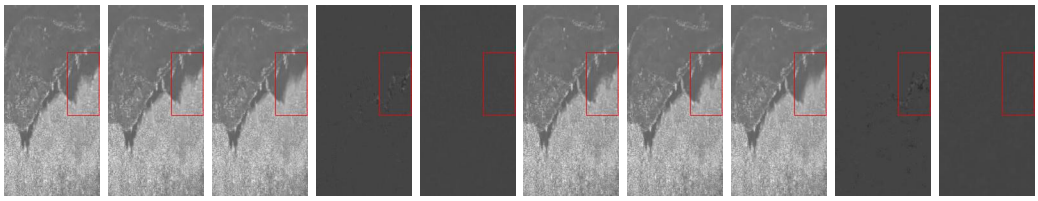


Figure 3: Low light video frame 30 for M0001, M0004, and M0009 ($\widehat{\boldsymbol{Z}} = \widehat{\boldsymbol{L}} + \widehat{\boldsymbol{S}} - \widehat{\boldsymbol{D}}$). Image contrast is enhanced using `imadjustn()` in Matlab.

4.4 Real Data with Natural Noise: Optical Coherence Tomography

In medical imaging, Optical Coherence Tomography can be used for micro-scale resolution, quick scanning of biological phenomenon [33]. These scans of the same scene over time, called time-lapse B-scan, are often noisy, but fit into our low rank/sparse model.

In this experiment, we apply $\sqrt{\text{PCP}}$ to the time-lapse B-scans (250 frames of resolution 300×150) of human trachea samples containing motile cilia (demo dataset of [33] under CC0 License). We present the recovered frame 50 and 100 in Figure 4. As expected, $\widehat{\boldsymbol{L}}$ captures the static background, and $\widehat{\boldsymbol{S}}$ captures the motion of cilia.



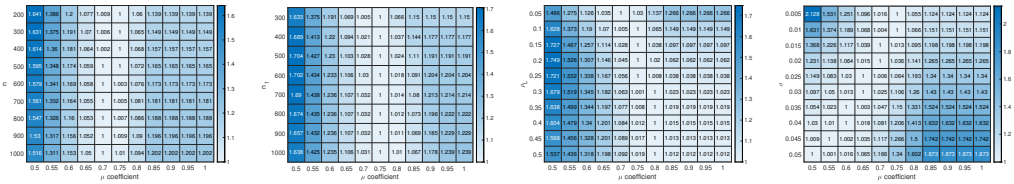
(a) $\boldsymbol{D}$ (b) $\widehat{\boldsymbol{L}}+\widehat{\boldsymbol{S}}$ (c) $\widehat{\boldsymbol{L}}$ (d) $\widehat{\boldsymbol{S}}$ (e) $\widehat{\boldsymbol{Z}}$ (f) $\boldsymbol{D}$ (g) $\widehat{\boldsymbol{L}}+\widehat{\boldsymbol{S}}$ (h) $\widehat{\boldsymbol{L}}$ (i) $\widehat{\boldsymbol{S}}$ (j) $\widehat{\boldsymbol{Z}}$

Figure 4: OCT, a-e): frame 50, f-j): frame 100 ($\widehat{\boldsymbol{Z}} = \widehat{\boldsymbol{L}} + \widehat{\boldsymbol{S}} - \widehat{\boldsymbol{D}}$).

4.5 Optimal Choice of μ

Our main result Theorem 1.1 suggests a tuning-free $\mu = \sqrt{n_2/2}$. Here, we investigate experimentally if this choice of μ is optimal. We vary the problem dimensions n_1 and n_2, the rank-dimension ratio $\rho_L := r/n$ ($n = n_1 = n_2$), and the noise standard deviation σ. For each choice of parameters $(n_1, n_2, \rho_L, \sigma)$, we generate 10 pairs of $(\boldsymbol{L}_0, \boldsymbol{S}_0, \boldsymbol{Z}_0)$ using the same method as in Section 4.1, run $\sqrt{\text{PCP}}$ with $\lambda = 1/\sqrt{n_1}$ and $\mu = c\mu_0$, where $\mu_0 = \sqrt{n_2}$ and c is a varying coefficient ($c = 1/\sqrt{2} \approx 0.71$ corresponds to our proposed value). Settings of all parameters are included in the supplementary material.

We use the 10-average of $\|(\widehat{\boldsymbol{L}}, \widehat{\boldsymbol{S}}) - (\boldsymbol{L}_0, \boldsymbol{S}_0)\|_F$ as the evaluation metric. In Figure 5, we show the heatmaps of this metric relative to the optimal $\mu = c\mu_0$ among all tested c, i.e. $\eta_{\text{rel}}(\mu) = \frac{\|(\widehat{\boldsymbol{L}}(\mu), \widehat{\boldsymbol{S}}(\mu)) - (\boldsymbol{L}_0, \boldsymbol{S}_0)\|_F}{\min_{\mu' = c\mu_0} \|(\widehat{\boldsymbol{L}}(\mu'), \widehat{\boldsymbol{S}}(\mu')) - (\boldsymbol{L}_0, \boldsymbol{S}_0)\|_F}$, so the optimal μ has value 1 in each row of the heatmaps. From Figure 5, we see that varying n_1, n_2 has little effect on the optimal choice



(a) vary $n = n_1 = n_2$ (b) vary n_1 (c) vary ρ_L (d) vary σ

Figure 5: $\eta_{\text{rel}}(\mu)$ under different varying parameters

of μ, which is approximately between $0.7\sqrt{n_2}$ and $0.75\sqrt{n_2}$, close to our $\sqrt{n_2/2}$. However, decreasing ρ_L or increasing σ suggests a smaller value of optimal μ. This makes sense because with higher level of noise or smaller rank (thus smaller norm $\|\boldsymbol{L}_0\|_F$), the SNR is smaller, so we should put smaller penalty on $\|\boldsymbol{L} + \boldsymbol{S} - \boldsymbol{D}\|_F$. Nevertheless, in all these settings, choosing $\mu = \sqrt{n_2/2}$ still gives satisfying results, as the recovery errors for $\mu = 0.7\sqrt{n_2}$ are close to the optimal performance: the error ratios are below 1.2. From these results, we believe that while $\mu = \sqrt{n_2/2}$ may not be the optimal choice with respect to the recovery error, it can provide performance close to the optimal, and is therefore a very effective choice.

5 Conclusion

In this work, we propose $\sqrt{\text{PCP}}$, a convex optimization approach for noisy robust low-rank matrix recovery. The benefit of our approach as compared to previous methods such as stable PCP is that it enables tuning-free recovery of low-rank matrices: theoretical analysis and simulations show that a single universal penalty parameter yields stable recovery at any noise standard deviation. Real video data experiments show suggest that many real life models fit into this low-rank plus sparse setting, and $\sqrt{\text{PCP}}$ (as well as stable PCP) does a good job in denosing and recovering the patterns of interest.

The presented experiments suggest the potential for both positive and negative societal impacts: visual surveillance can be abused, leading to significant negative impacts; at the same time, the denoising and foreground/background separation ability of $\sqrt{\text{PCP}}$ can help improve the quality of noisy data in biomedical and scientific research (e.g. medical imaging), and people's life (e.g. low light video).

Acknowledgement

We would like to thank Marianthi-Anna Kioumourtzoglou, Jeff Goldsmith, Elizabeth Gibson, Rachel Tao and Lawrence Chillrud for many helpful discussions around matrix modeling of environmental data and the need for tuning-free solutions. This work was partially funded by the National Institute of Environmental Health Sciences (NIEHS) grant R01 ES028805. We also thank Christine Hendon for helpful pointers regarding optical coherence tomography data. Jingkai Yan also gratefully acknowledges support from the Wei Family Foundation.

References

[1] Xiaoyuan Su and Taghi M Khoshgoftaar. A survey of collaborative filtering techniques. *Advances in artificial intelligence*, 2009, 2009.

[2] Thomas Hofmann. Probabilistic latent semantic indexing. In *Proceedings of the 22nd annual international ACM SIGIR conference on Research and development in information retrieval*, pages 50–57, 1999.

[3] Benjamin Haeffele, Eric Young, and Rene Vidal. Structured low-rank matrix factorization: Optimality, algorithm, and applications to image processing. In *International conference on machine learning*, pages 2007–2015. PMLR, 2014.

[4] Hongyan Zhang, Wei He, Liangpei Zhang, Huanfeng Shen, and Qiangqiang Yuan. Hyperspectral image restoration using low-rank matrix recovery. *IEEE transactions on geoscience and remote sensing*, 52(8):4729–4743, 2013.

[5] Hui Ji, Chaoqiang Liu, Zuowei Shen, and Yuhong Xu. Robust video denoising using low rank matrix completion. In *2010 IEEE Computer Society Conference on Computer Vision and Pattern Recognition*, pages 1791–1798. IEEE, 2010.

[6] Emmanuel J Candès, Xiaodong Li, Yi Ma, and John Wright. Robust principal component analysis? *Journal of the ACM (JACM)*, 58(3):1–37, 2011.

[7] Praneeth Netrapalli, UN Niranjan, Sujay Sanghavi, Animashree Anandkumar, and Prateek Jain. Non-convex robust pca. *arXiv preprint arXiv:1410.7660*, 2014.

[8] Yuxin Chen, Jianqing Fan, Cong Ma, and Yuling Yan. Bridging convex and nonconvex optimization in robust pca: Noise, outliers, and missing data. *arXiv preprint arXiv:2001.05484*, 2020.

[9] Zihan Zhou, Xiaodong Li, John Wright, Emmanuel Candes, and Yi Ma. Stable principal component pursuit. In *2010 IEEE international symposium on information theory*, pages 1518–1522. IEEE, 2010.

[10] Yudong Chen and Martin J Wainwright. Fast low-rank estimation by projected gradient descent: General statistical and algorithmic guarantees. *arXiv preprint arXiv:1509.03025*, 2015.

[11] Alexandre Belloni, Victor Chernozhukov, and Lie Wang. Square-root lasso: pivotal recovery of sparse signals via conic programming. *Biometrika*, 98(4):791–806, 2011.

[12] Stephen Boyd, Neal Parikh, Eric Chu, Borja Peleato, and Jonathan Eckstein. Distributed optimization and statistical learning via the alternating direction method of multipliers. *Found. Trends Mach. Learn.*, 3(1):1–122, January 2011.

[13] Venkat Chandrasekaran, Sujay Sanghavi, Pablo A Parrilo, and Alan S Willsky. Rank-sparsity incoherence for matrix decomposition. *SIAM Journal on Optimization*, 21(2):572–596, 2011.

[14] Daniel Hsu, Sham M Kakade, and Tong Zhang. Robust matrix decomposition with outliers. *arXiv preprint arXiv:1011.1518*, 2010.

[15] Xiaodong Li. Compressed sensing and matrix completion with constant proportion of corruptions. *Constructive Approximation*, 37(1):73–99, 2013.

[16] Yudong Chen, Ali Jalali, Sujay Sanghavi, and Constantine Caramanis. Low-rank matrix recovery from errors and erasures. *IEEE Transactions on Information Theory*, 59(7):4324–4337, 2013.

[17] Quanquan Gu, Zhaoran Wang Wang, and Han Liu. Low-rank and sparse structure pursuit via alternating minimization. In *Artificial Intelligence and Statistics*, pages 600–609. PMLR, 2016.

[18] Rong Ge, Chi Jin, and Yi Zheng. No spurious local minima in nonconvex low rank problems: A unified geometric analysis. In *International Conference on Machine Learning*, pages 1233–1242. PMLR, 2017.

[19] Chong You, Zhihui Zhu, Qing Qu, and Yi Ma. Robust recovery via implicit bias of discrepant learning rates for double over-parameterization, 2020.

[20] Alekh Agarwal, Sahand Negahban, Martin J Wainwright, et al. Noisy matrix decomposition via convex relaxation: Optimal rates in high dimensions. *The Annals of Statistics*, 40(2):1171–1197, 2012.

[21] Olga Klopp, Karim Lounici, and Alexandre B Tsybakov. Robust matrix completion. *Probability Theory and Related Fields*, 169(1):523–564, 2017.

[22] Raymond KW Wong and Thomas CM Lee. Matrix completion with noisy entries and outliers. *The Journal of Machine Learning Research*, 18(1):5404–5428, 2017.

[23] Florentina Bunea, Johannes Lederer, and Yiyuan She. The group square-root lasso: Theoretical properties and fast algorithms. *IEEE Transactions on Information Theory*, 60(2):1313–1325, 2013.

[24] Alexis Derumigny et al. Improved bounds for square-root lasso and square-root slope. *Electronic Journal of Statistics*, 12(1):741–766, 2018.

[25] Elias Raninen and Esa Ollila. Scaled and square-root elastic net. In *2017 IEEE International Conference on Acoustics, Speech and Signal Processing (ICASSP)*, pages 4336–4340. IEEE, 2017.

[26] Olga Klopp et al. Noisy low-rank matrix completion with general sampling distribution. *Bernoulli*, 20(1):282–303, 2014.

[27] Xinyue Shen, Laming Chen, Yuantao Gu, and H. C. So. Square-root lasso with nonconvex regularization: An admm approach. *IEEE Signal Processing Letters*, 23(7):934–938, 2016.

[28] Xingguo Li, Tuo Zhao, Xiaoming Yuan, and Han Liu. The flare package for high dimensional linear regression and precision matrix estimation in r. *Journal of Machine Learning Research*, 16(18):553–557, 2015.

[29] Caihua Chen, Bingsheng He, Yinyu Ye, and Xiaoming Yuan. The direct extension of admm for multi-block convex minimization problems is not necessarily convergent. *Math. Program.*, 155(1–2):57–79, January 2016.

[30] Liyuan Li, Weimin Huang, Irene Yu-Hua Gu, and Qi Tian. Statistical modeling of complex backgrounds for foreground object detection. *IEEE Transactions on Image Processing*, 13(11):1459–1472, 2004.

[31] Roman Vershynin. *Introduction to the non-asymptotic analysis of random matrices*, page 210–268. Cambridge University Press, 2012.

[32] Chen Chen, Qifeng Chen, Minh Do, and Vladlen Koltun. Seeing motion in the dark. In *2019 IEEE/CVF International Conference on Computer Vision (ICCV)*, pages 3184–3193, 2019.

[33] James P. McLean, Yuye Ling, and Christine P. Hendon. Frequency-constrained robust principal component analysis: a sparse representation approach to segmentation of dynamic features in optical coherence tomography imaging. *Opt. Express*, 25(21):25819–25830, Oct 2017.

[34] A.S. Georghiades, P.N. Belhumeur, and D.J. Kriegman. From few to many: Illumination cone models for face recognition under variable lighting and pose. *IEEE Trans. Pattern Anal. Mach. Intelligence*, 23(6):643–660, 2001.

A Proof of Lemma 2.2 and Main Theorem 1.1

Proof [Lemma 2.2] Clearly, $\widehat{\boldsymbol{L}}_{\rm root}(\mu), \widehat{\boldsymbol{S}}_{\rm root}(\mu)$ satisfies the constraint for the StablePCP$_c$ with $\delta = \delta(\mu)$. And by optimality of $\widehat{\boldsymbol{L}}_{\rm root}(\mu), \widehat{\boldsymbol{S}}_{\rm root}(\mu)$ for the $\sqrt{\rm PCP}$ problem, we get $\forall \boldsymbol{L}, \boldsymbol{S}\ s.t. \|\boldsymbol{D} - \boldsymbol{L} - \boldsymbol{S}\|_F \le \delta(\mu)$,

$$\|\boldsymbol{L}\|_* + \lambda\|\boldsymbol{S}\|_1 \ge \|\widehat{\boldsymbol{L}}_{\rm root}(\mu)\|_* + \lambda\|\widehat{\boldsymbol{S}}_{\rm root}(\mu)\|_1. \tag{A.1}$$

This shows the optimality of $\widehat{\boldsymbol{L}}_{\rm root}(\mu), \widehat{\boldsymbol{S}}_{\rm root}(\mu)$ for the StablePCP$_c$ problem with $\delta = \delta(\mu)$. ■

Lemma A.1 (Adapted from Theorem 2 in [9]) *Under the same conditions as Theorem 2.1, with probability at least $1 - c' n_1^{-10}$, for any $\boldsymbol{Z}_0$ with $\|\boldsymbol{Z}_0\|_F \ge \delta$, the solution $\widehat{\boldsymbol{X}} = (\widehat{\boldsymbol{L}}, \widehat{\boldsymbol{S}})$ to the StablePCP$_c$ problem 1.5 with $\lambda = 1/\sqrt{n_1}$ satisfies*

$$\|\widehat{\boldsymbol{X}} - \boldsymbol{X}_0\|_F \le \sqrt{720 n_1 n_2 + 2} \cdot \|\boldsymbol{Z}_0\|_F.$$

The proof of this lemma is essentially the same as the proof of Theorem 2.1 in [9]. The main differences are: we need to replace every occurrence of δ with $\|\boldsymbol{Z}_0\|_F$, and now since $(\widehat{\boldsymbol{L}_0}, \widehat{\boldsymbol{S}_0})$ is not a feasible solution, we need to change the bound of the objective to $\|\widehat{\boldsymbol{L}}\|_* + \lambda\|\widehat{\boldsymbol{S}}\|_1 \le \|\widehat{\boldsymbol{L}} + \widehat{\boldsymbol{Z}_0}\|_* + \lambda\|\widehat{\boldsymbol{S}}\|_1 \le \|\widehat{\boldsymbol{L}}\|_* + \sqrt{n_2}\|\boldsymbol{Z}_0\|_F + \lambda\|\widehat{\boldsymbol{S}}\|_1$.

Proof [Theorem 1.1] Define $\widehat{\boldsymbol{\delta}_L} = \widehat{\boldsymbol{L}} - \boldsymbol{L}_0$ and $\widehat{\boldsymbol{\delta}_S} = \widehat{\boldsymbol{S}} - \boldsymbol{S}_0$. By the optimality of $\widehat{\boldsymbol{L}}, \widehat{\boldsymbol{S}}$ and triangle inequality,

$$\begin{aligned}
&(\|\boldsymbol{L}_0\|_* + \lambda\|\boldsymbol{S}_0\|_1) - (\|\widehat{\boldsymbol{L}}\|_* + \lambda\|\widehat{\boldsymbol{S}}\|_1) \\
&\ge \mu(\|\boldsymbol{D} - \widehat{\boldsymbol{L}} - \widehat{\boldsymbol{S}}\|_F - \|\boldsymbol{Z}_0\|_F) \\
&\ge \mu(\|\widehat{\boldsymbol{\delta}_L} + \widehat{\boldsymbol{\delta}_S}\|_F - 2\|\boldsymbol{Z}_0\|_F).
\end{aligned} \tag{A.2}$$

Treating the dual certificate in Lemma 2.3 as an approximate subgradient for the norm $\|\cdot\|_*$ and $\|\cdot\|_1$,

$$\begin{aligned}
&(\|\widehat{\boldsymbol{L}}\|_* - \|\boldsymbol{L}_0\|_*) + \lambda(\|\widehat{\boldsymbol{S}}\|_1 - \|\boldsymbol{S}_0\|_1) \\
&\ge \langle \widehat{\boldsymbol{\delta}_L}, \boldsymbol{U}\boldsymbol{V}^* + \boldsymbol{W}\rangle + \langle \widehat{\boldsymbol{\delta}_S}, \lambda(\operatorname{sign}(\boldsymbol{S}_0) + \boldsymbol{F})\rangle \\
&= \underbrace{\left\langle \widehat{\boldsymbol{\delta}_L} + \widehat{\boldsymbol{\delta}_S}, \boldsymbol{U}\boldsymbol{V}^* + \boldsymbol{W} - \frac{\lambda P_\Omega \boldsymbol{H}}{2} \right\rangle}_{\Theta_1} + \underbrace{\lambda \left\langle \widehat{\boldsymbol{\delta}_L} - \widehat{\boldsymbol{\delta}_S}, \frac{P_\Omega \boldsymbol{H}}{2} \right\rangle}_{\Theta_2}.
\end{aligned} \tag{A.3}$$

Next, we bound Θ_1, Θ_2 in (A.3).

$$\begin{aligned}
\Theta_1 &\ge -\|\widehat{\boldsymbol{\delta}_L} + \widehat{\boldsymbol{\delta}_S}\|_F \cdot \|\boldsymbol{U}\boldsymbol{V}^* + \boldsymbol{W} - \lambda P_\Omega \boldsymbol{H}/2\|_F \\
&\ge -\|\widehat{\boldsymbol{\delta}_L} + \widehat{\boldsymbol{\delta}_S}\|_F \cdot (\sqrt{r + n_2/4} + \lambda\|P_\Omega \boldsymbol{H}\|_F/2) \\
&\ge -\|\widehat{\boldsymbol{\delta}_L} + \widehat{\boldsymbol{\delta}_S}\|_F \cdot (\sqrt{7/10} + 1/520)\sqrt{n_2/2} \\
&\ge -0.85\mu\|\widehat{\boldsymbol{\delta}_L} + \widehat{\boldsymbol{\delta}_S}\|_F.
\end{aligned}$$

where the second inequality follows from triangle inequality and properties of $\boldsymbol{W}$ from Lemma 2.3. The third inequality follows from the condition (1.3) $r \le n_2/10$. For Θ_2, by the dual construction,

$$\Theta_2 \ge -(\lambda\|P_\Omega \boldsymbol{H}\|_F/2) \cdot (\|\widehat{\boldsymbol{\delta}_L}\|_F + \|\widehat{\boldsymbol{\delta}_S}\|_F) \ge -(\|\widehat{\boldsymbol{\delta}_L}\|_F + \|\widehat{\boldsymbol{\delta}_S}\|_F)/(520\sqrt{2n_1}).$$

Combining (A.2) and (A.3) with the bounds on Θ_1 and Θ_2,

$$\frac{1}{520\sqrt{n_1 n_2}}(\|\widehat{\boldsymbol{\delta}_L}\|_F + \|\widehat{\boldsymbol{\delta}_S}\|_F) + 2\|\boldsymbol{Z}_0\|_F \ge 0.15\|\widehat{\boldsymbol{\delta}_L} + \widehat{\boldsymbol{\delta}_S}\|_F. \tag{A.4}$$

From Lemma 2.2, $(\widehat{\boldsymbol{L}}, \widehat{\boldsymbol{S}})$ is also the solution to the StablePCP$_c$ problem parameterized by $\delta = \|\widehat{\boldsymbol{\delta}_L} + \widehat{\boldsymbol{\delta}_S} - \boldsymbol{Z}_0\|_F$. If $\delta \le \|\boldsymbol{Z}_0\|_F$, Lemma A.1 gives the bound that

$$\|(\widehat{\boldsymbol{\delta}_L}, \widehat{\boldsymbol{\delta}_S})\|_F \le 27\sqrt{n_1 n_2}\|\boldsymbol{Z}_0\|_F.$$

If $\delta \geq \|\boldsymbol{Z}_0\|_F$, from Theorem 2.1, together with the trivial inequality that $\sqrt{320n_1n_2+4} \leq 26\sqrt{n_1n_2/2}$,

$$\|(\widehat{\boldsymbol{\delta}_L}, \widehat{\boldsymbol{\delta}_S})\|_F \leq 26\sqrt{n_1n_2/2} \cdot \|\widehat{\boldsymbol{\delta}_L} + \widehat{\boldsymbol{\delta}_S} - \boldsymbol{Z}_0\|_F. \tag{A.5}$$

Combining (A.4) and (A.5), we get

$$\|\widehat{\boldsymbol{\delta}_L}\|_F + \|\widehat{\boldsymbol{\delta}_S}\|_F \leq 26\sqrt{n_1n_2}(\|\widehat{\boldsymbol{\delta}_L} + \widehat{\boldsymbol{\delta}_S}\|_F + \|\boldsymbol{Z}_0\|_F) \leq \frac{1}{3}(\|\widehat{\boldsymbol{\delta}_L}\|_F + \|\widehat{\boldsymbol{\delta}_S}\|_F) + 373\sqrt{n_1n_2}\|\boldsymbol{Z}_0\|_F.$$

which proves the claim that

$$\|\widehat{\boldsymbol{X}} - \boldsymbol{X}_0\|_F \leq \|\widehat{\boldsymbol{\delta}_L}\|_F + \|\widehat{\boldsymbol{\delta}_S}\|_F \leq 560\sqrt{n_1n_2}\|\boldsymbol{Z}_0\|_F.$$

■

B Stopping Criteria in Algorithm 1

The function `helper()` containing the stopping criteria and updates for ρ, adapted from [12], is presented in Algorithm 2.

Algorithm 2 Function `helper()`: update ρ and check convergence

Input: $\boldsymbol{D}, \boldsymbol{L}_1, \boldsymbol{L}_2, \boldsymbol{L}_2', \boldsymbol{S}_1, \boldsymbol{S}_2, \boldsymbol{S}_2', \boldsymbol{Z}, \boldsymbol{Y}_1, \boldsymbol{Y}_2, \boldsymbol{Y}_3 \in \mathbb{R}^{n_1 \times n_2}, \rho, \epsilon_{\text{abs}}, \epsilon_{\text{rel}}$.
Output: ρ_+, ifConverge.

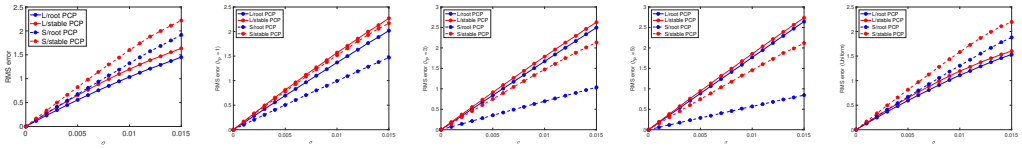
 # Calculate residuals
$r_{\text{primal}} \leftarrow \|(\boldsymbol{L}_1 - \boldsymbol{L}_2, \boldsymbol{S}_1 - \boldsymbol{S}_2, \boldsymbol{Z} + \boldsymbol{L}_2 + \boldsymbol{S}_2 - \boldsymbol{D})\|_F$
$r_{\text{dual}} \leftarrow \rho \cdot \|(\boldsymbol{L}_2 - \boldsymbol{L}_2', \boldsymbol{S}_2 - \boldsymbol{S}_2', \boldsymbol{L}_2 + \boldsymbol{S}_2 - \boldsymbol{L}_2' - \boldsymbol{S}_2')\|_F$
 # Calculate thresholds
$\theta_{\text{primal}} \leftarrow \epsilon_{\text{rel}} \max\{\|(\boldsymbol{L}_1, \boldsymbol{S}_1, \boldsymbol{Z})\|_F, \|(\boldsymbol{L}_2, \boldsymbol{S}_2, \boldsymbol{L}_2 + \boldsymbol{S}_2)\|_F, \|\boldsymbol{D}\|_F\} + \epsilon_{\text{abs}}\sqrt{3n_1n_2}$
$\theta_{\text{dual}} \leftarrow \epsilon_{\text{rel}}\|(\boldsymbol{Y}_1, \boldsymbol{Y}_2, \boldsymbol{Y}_3)\|_F + \epsilon_{\text{abs}}\sqrt{3n_1n_2}$
 # Update ρ
$\rho_+ \leftarrow \rho$
if $r_{\text{primal}} > 10 \cdot r_{\text{dual}}$ **then**
  $\rho_+ \leftarrow 2\rho$
else if $r_{\text{dual}} > 10 \cdot r_{\text{primal}}$ **then**
  $\rho_+ \leftarrow \rho/2$
end if
 # Check convergence
ifConverge $\leftarrow$ False
if $r_{\text{primal}} < \theta_{\text{primal}}$ and $r_{\text{dual}} < \theta_{\text{dual}}$ **then**
  ifConverge $\leftarrow$ True
end if
return ρ_+, ifConverge

C Experiments and Settings

C.1 Experiments with Different Distributions of Noise for Section 4.1

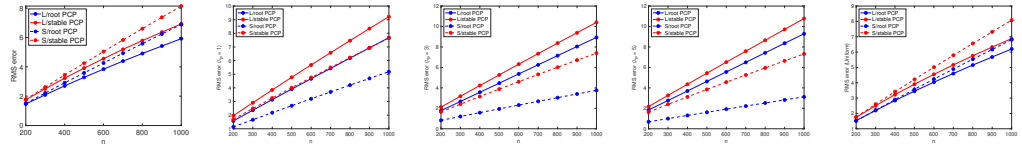
We test our $\sqrt{\text{PCP}}$ and StablePCP$_u$on simulation experiments with different noise distributions. All the setup and parameters are the same as in Section 4.1 except that now, instead of adding Gaussian noise which follows $\mathcal{N}(0, \sigma^2)$, we add (scaled) Poisson noise, $l \cdot Poisson(\lambda_P)$ where we choose $\lambda_P \in \{1, 3, 5\}$[7] with scale $l = \frac{\sigma}{\sqrt{\lambda_P + \lambda_P^2}}$, and Uniform noise $Uniform(-\sqrt{3}\sigma, \sqrt{3}\sigma)$. We choose (λ_P, l) and the range of the Uniform distribution in this way such that $E[(\boldsymbol{Z}_0)_{ij}^2] = \sigma^2$. Results are presented in Figures 6 and 7.

[7]Since a Poisson variable with parameter λ_P equals 0 with probability $e^{-\lambda_P}$, our choices of λ_P give $\boldsymbol{Z}_0$'s which are approximately 36.79%, 4.98%, and 0.67% sparse.



(a) Gaussian (b) Poisson $\lambda_P = 1$ (c) Poisson $\lambda_P = 3$ (d) Poisson $\lambda_P = 5$ (e) Uniform

Figure 6: StablePCP$_u$ vs $\sqrt{\text{PCP}}$: effect of varying σ for different noise distributions



(a) Gaussian (b) Poisson $\lambda_P = 1$ (c) Poisson $\lambda_P = 3$ (d) Poisson $\lambda_P = 5$ (e) Uniform

Figure 7: StablePCP$_u$ vs $\sqrt{\text{PCP}}$: effect of varying n for different noise distributions

C.2 Additional Results for Section 4.2

We run the experiments on a laptop with 2.3 GHz Dual-Core Intel Core i5, and we set the maximal iteration number of our ADMM to be 5000. For experiments that don't converge in 5000 steps, the number of iterations is represented as $5000+$.

For the hall dataset, we present the relative error for $\boldsymbol{L}$, $\boldsymbol{S}$, the running time, and the number of iteration in Table 1 and Table 2.

Table 1: $\sqrt{\text{PCP}}$: Hall dataset

σ	$\frac{\|\widehat{\boldsymbol{L}}-\boldsymbol{L}_0\|_F}{\|\boldsymbol{L}_0\|_F}$	$\frac{\|\widehat{\boldsymbol{S}}-\boldsymbol{S}_0\|_F}{\|\boldsymbol{S}_0\|_F}$	Time ($\times 10^3$ s)	Iter
0	0.0019	0.0266	0.6894	1688
30	0.0445	0.7403	0.5381	1293
60	0.0737	1.3525	0.9470	2425
90	0.0968	1.9288	1.4040	3258
120	0.1200	2.5067	1.6230	4113

Table 2: StablePCP$_u$: Hall dataset

σ	$\frac{\|\widehat{\boldsymbol{L}}-\boldsymbol{L}_0\|_F}{\|\boldsymbol{L}_0\|_F}$	$\frac{\|\widehat{\boldsymbol{S}}-\boldsymbol{S}_0\|_F}{\|\boldsymbol{S}_0\|_F}$	Time ($\times 10^3$ s)	Iter
0	0.0019	0.0266	1.7340	4423
30	0.0443	0.7495	1.8936	4918
60	0.0740	1.3494	1.3006	3362
90	0.0974	1.8922	1.8050	4563
120	0.1214	2.4349	1.9886	5000+

In Figure 8 and 9, we present more results for frame 1, 20 for varying σ for this hall dataset.

We also apply our algorithms to the dataset lights. We present the relative error for $\boldsymbol{L}$, $\boldsymbol{S}$, the running time, and the number of iteration in Table 3 and Table 4.

Table 3: $\sqrt{\text{PCP}}$: Lights dataset

σ	$\frac{\|\widehat{\boldsymbol{L}}-\boldsymbol{L}_0\|_F}{\|\boldsymbol{L}_0\|_F}$	$\frac{\|\widehat{\boldsymbol{S}}-\boldsymbol{S}_0\|_F}{\|\boldsymbol{S}_0\|_F}$	Time ($\times 10^3$ s)	Iter
0	0.0013	0.1052	0.7100	1605
30	0.0520	2.9707	0.5120	1155
60	0.0938	5.8908	1.7101	3880
90	0.1323	8.7761	2.1983	5000+
120	0.1689	11.5848	2.5344	5000+

Table 4: StablePCP$_u$: Lights dataset

σ	$\frac{\|\widehat{\boldsymbol{L}}-\boldsymbol{L}_0\|_F}{\|\boldsymbol{L}_0\|_F}$	$\frac{\|\widehat{\boldsymbol{S}}-\boldsymbol{S}_0\|_F}{\|\boldsymbol{S}_0\|_F}$	Time ($\times 10^3$ s)	Iter
0	0.0013	0.1052	2.2069	5000+
30	0.0527	2.7920	1.4677	3377
60	0.0951	5.5085	1.2136	2804
90	0.1342	8.2023	1.6699	3886
120	0.1710	10.8930	2.0856	4902

In Figure 10 and 11, we present more results for frame 1, 20 for varying σ for this lights dataset.

In Figure 12(a), we present the RMS error. Again, we see that the error is linear in the noise level σ.

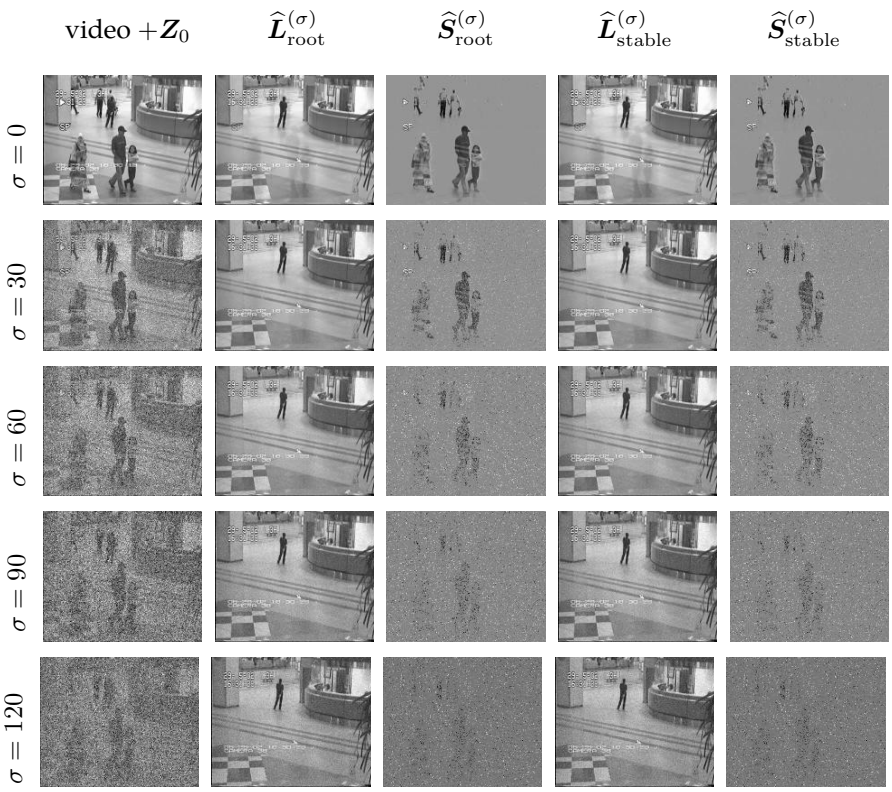


Figure 8: hall: recovered $\widehat{\boldsymbol{L}}$, $\widehat{\boldsymbol{S}}$ for frame 1

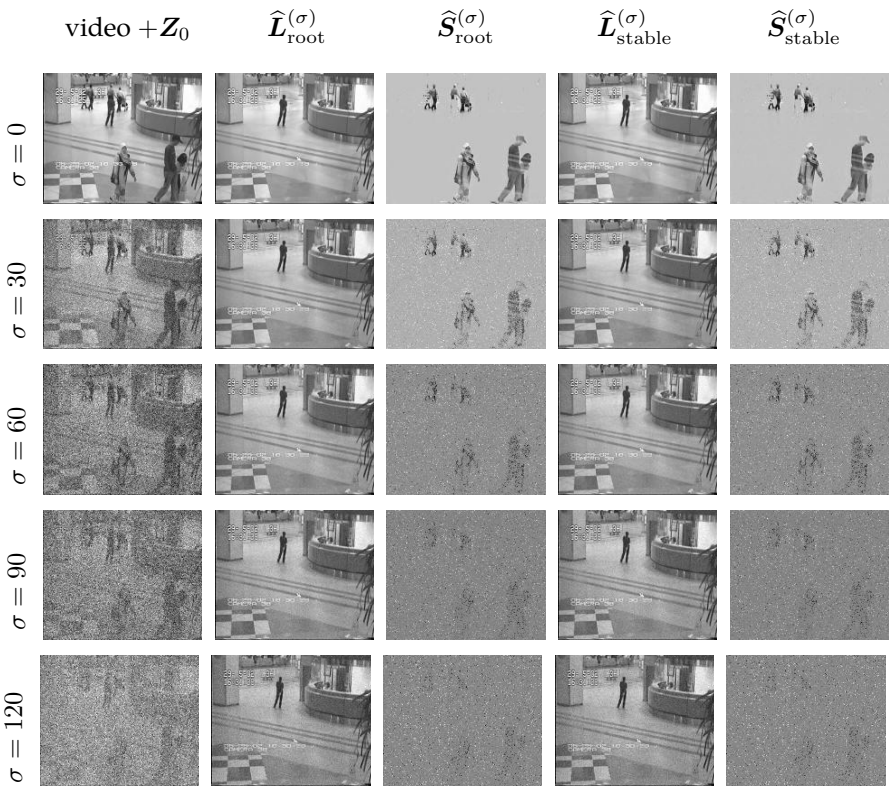


Figure 9: hall: recovered $\widehat{\boldsymbol{L}}$, $\widehat{\boldsymbol{S}}$ for frame 20

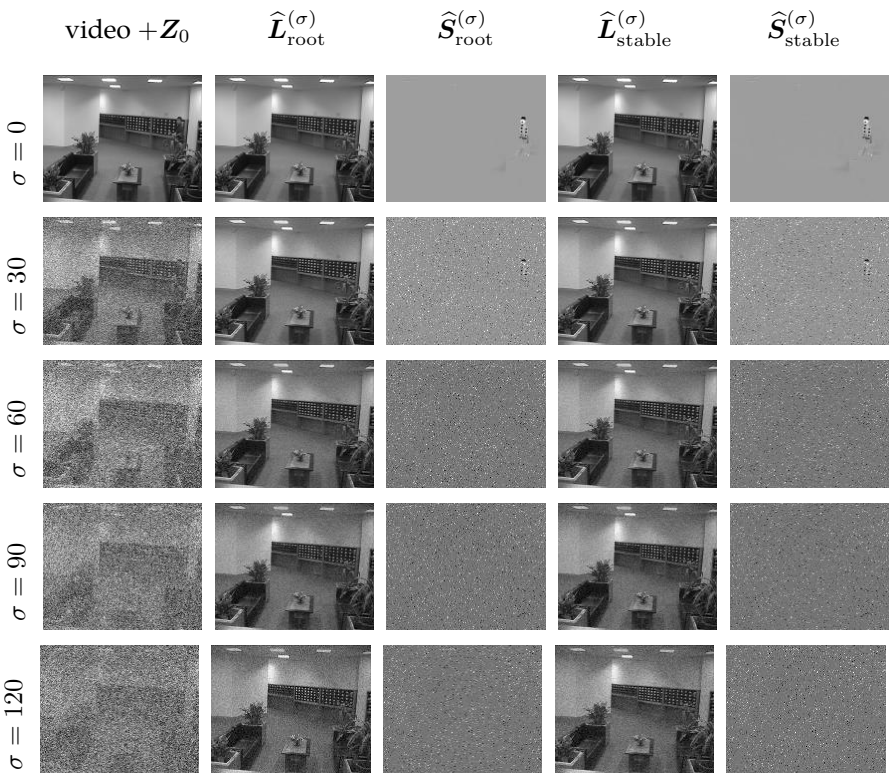


Figure 10: lights: recovered $\widehat{\boldsymbol{L}}$, $\widehat{\boldsymbol{S}}$ for frame 1

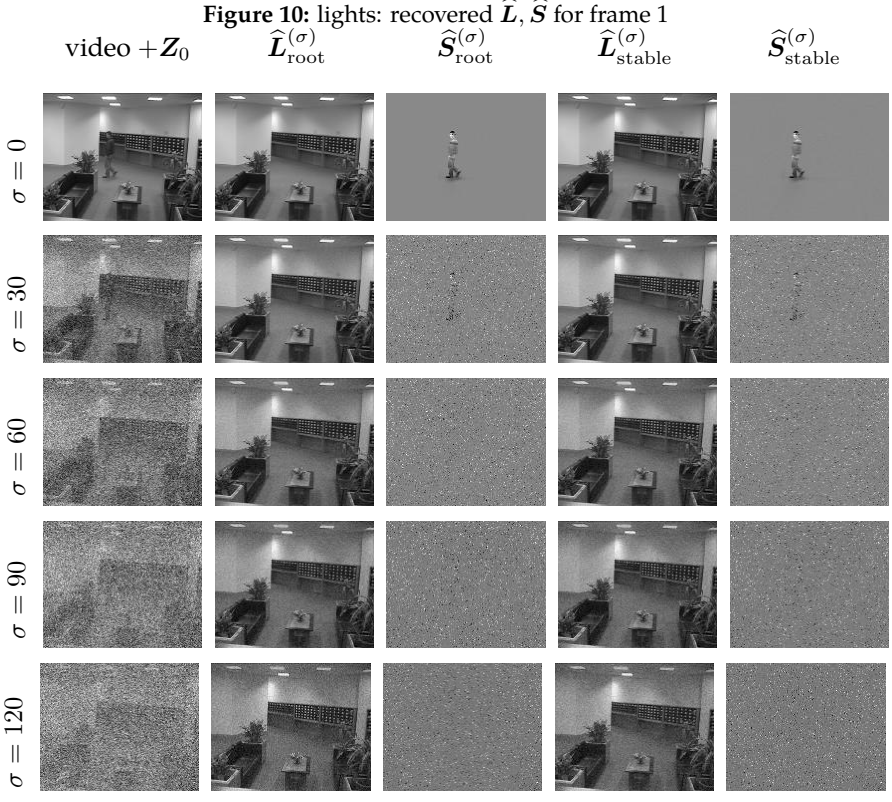
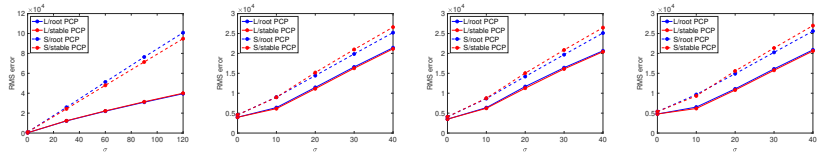


Figure 11: lights: recovered $\widehat{\boldsymbol{L}}$, $\widehat{\boldsymbol{S}}$ for frame 20

C.3 Additional Experiments Using Face Dataset

In addition to the video dataset in the previous section, we also test $\sqrt{\text{PCP}}$ and StablePCP$_u$ on datasets of face images. It has been pointed out in [6] that under distant illumination,



(a) "lights"+noise (b) yaleB01 + noise (c) yaleB02 + noise (d) yaleB03 + noise

Figure 12: StablePCP$_u$ vs $\sqrt{\text{PCP}}$: real datasets

images of a convex Lambertian object lie near a low dimensional linear subspace called the *harmonic plane*. However, real images of faces are often corrupted by shadows and specularities, which can have large magnitudes but are sparse in the spatial domain. This fits well into our low-rank and sparse model [8], and our goal is to remove these shadows and specularities from the noisy and corrupted observation.

To be precise, the dataset we use is from Yale B face database [34]. For each face, there are 65 images of resolution 192×168 under various illuminations, so we have $n_1 = 192 \times 168 = 32256$ and $n_2 = 65$. Similar to the experiments on the video dataset, we assume that there is no noise in these images, and add $\boldsymbol{Z}_0$ with $\sigma \in \{0, 10, 20, 30, 40\}$.

In Figures 13, 14, 15, 16, 17, and 18, we present the recovered low rank and sparse matrices for frame 1 and frame 20 using $\sqrt{\text{PCP}}$ and StablePCP$_u$.

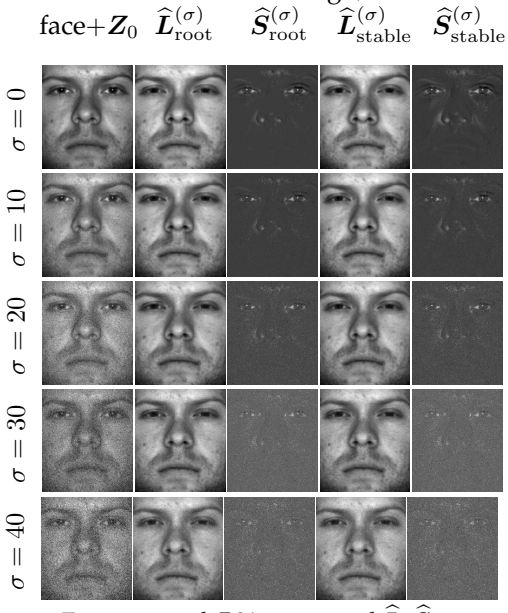


Figure 13: yaleB01: recovered $\widehat{\boldsymbol{L}}, \widehat{\boldsymbol{S}}$ for frame 1

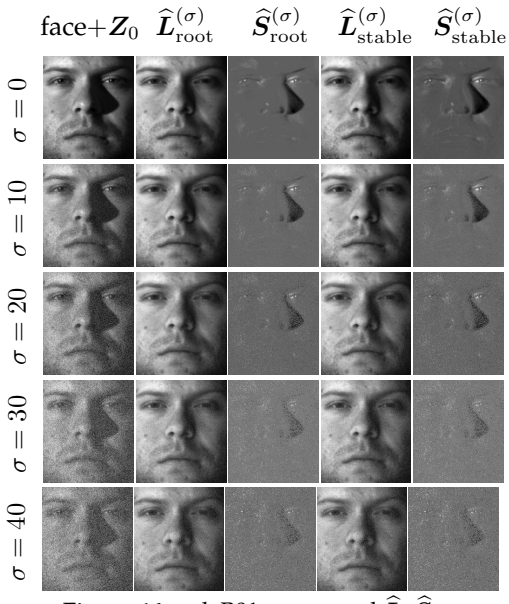


Figure 14: yaleB01: recovered $\widehat{\boldsymbol{L}}, \widehat{\boldsymbol{S}}$ for frame 20

In Table 5, 7, and 9, we show the relative error, running time and iteration for $\sqrt{\text{PCP}}$ on yaleB01, yaleB02, and yaleB03 datasets. In Table 6, 8, and 10, we show the relative error, running time and iteration for StablePCP$_u$on yaleB01, yaleB02, and yaleB03 datasets.

C.4 Additional Results for Section 4.3

We provide frame 30, 60, and 90 for the three videos in Figures 19, 20, and 21.

C.5 Additional Results for Section 4.4

Results for frame 150 and 200 are presented in Figure 22.

[8] Although faces are not convex Lambertian objects and the harmonic plane may not apply here, previous experiments in [6] have shown the effectiveness of PCP in this task.

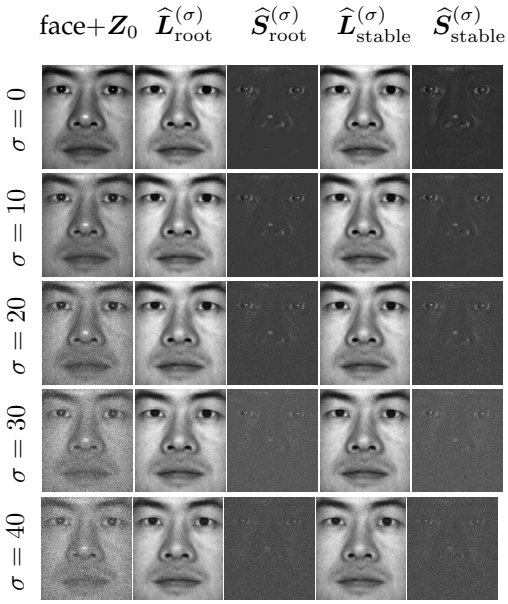


Figure 15: yaleB02: recovered $\widehat{L}, \widehat{S}$ for frame 1

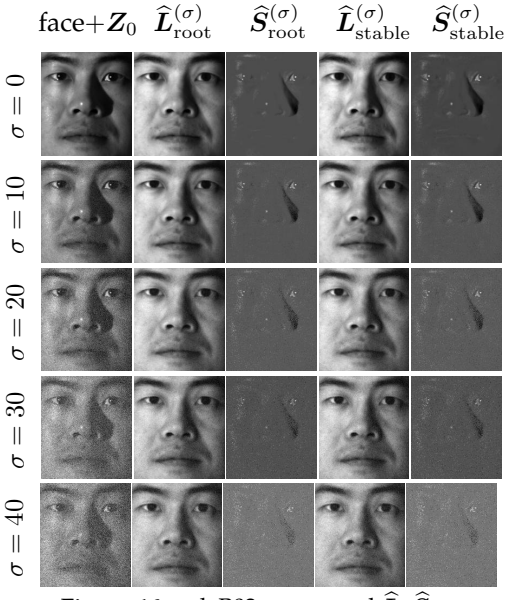


Figure 16: yaleB02: recovered $\widehat{L}, \widehat{S}$ for frame 20

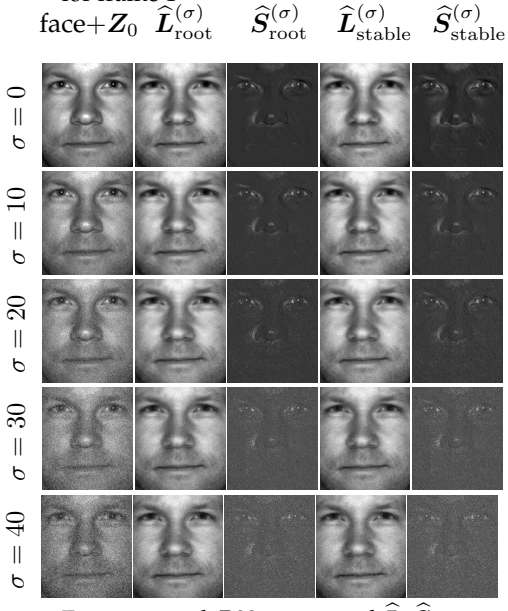


Figure 17: yaleB03: recovered $\widehat{L}, \widehat{S}$ for frame 1

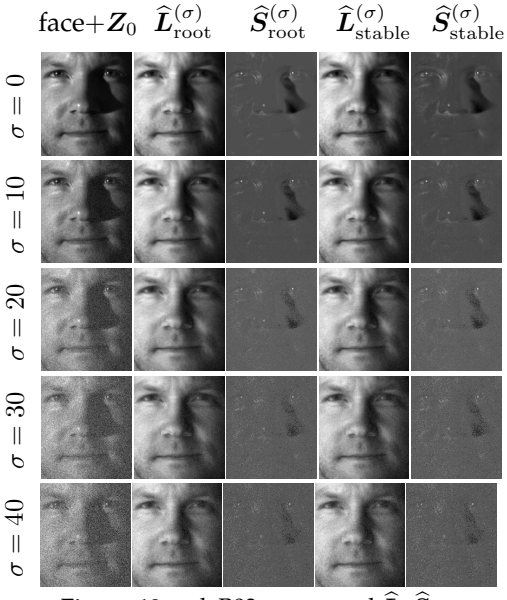


Figure 18: yaleB03: recovered $\widehat{L}, \widehat{S}$ for frame 20

Table 5: $\sqrt{\text{PCP}}$: yaleB01

σ	$\frac{\|\widehat{L}-L_0\|_F}{\|L_0\|_F}$	$\frac{\|\widehat{S}-S_0\|_F}{\|S_0\|_F}$	Time (s)	Iter
0	0.0298	0.1934	255.6449	2054
10	0.0481	0.3823	171.0386	1366
20	0.0863	0.6117	184.6412	1480
30	0.1250	0.8421	210.4474	1693
40	0.1613	1.0692	493.5861	3953

Table 6: StablePCP$_u$: yaleB01

σ	$\frac{\|\widehat{L}-L_0\|_F}{\|L_0\|_F}$	$\frac{\|\widehat{S}-S_0\|_F}{\|S_0\|_F}$	Time (s)	Iter
0	0.0298	0.1934	602.0781	5000+
10	0.0461	0.3808	599.3534	5000+
20	0.0838	0.6441	594.2583	5000+
30	0.1225	0.8898	596.9568	5000+
40	0.1591	1.1276	602.5028	5000+

C.6 Settings and Additional Results for Section 4.5

Table 11 below lists the settings for this set of experiments.

Table 7: $\sqrt{\text{PCP}}$: yaleB02

σ	$\frac{\|\widehat{\boldsymbol{L}}-\boldsymbol{L}_0\|_F}{\|\boldsymbol{L}_0\|_F}$	$\frac{\|\widehat{\boldsymbol{S}}-\boldsymbol{S}_0\|_F}{\|\boldsymbol{S}_0\|_F}$	Time (s)	Iter
0	0.0261	0.1720	272.5150	2190
10	0.0477	0.3657	167.7344	1352
20	0.0873	0.5993	174.0215	1409
30	0.1228	0.8311	407.7892	3289
40	0.1545	1.0599	244.3114	1970

Table 8: StablePCP$_u$: yaleB02

σ	$\frac{\|\widehat{\boldsymbol{L}}-\boldsymbol{L}_0\|_F}{\|\boldsymbol{L}_0\|_F}$	$\frac{\|\widehat{\boldsymbol{S}}-\boldsymbol{S}_0\|_F}{\|\boldsymbol{S}_0\|_F}$	Time (s)	Iter
0	0.0261	0.1720	595.5254	5000+
10	0.0465	0.3697	595.0926	5000+
20	0.0843	0.6348	594.2518	5000+
30	0.1204	0.8808	599.8056	5000+
40	0.1528	1.1174	593.7441	5000+

Table 9: $\sqrt{\text{PCP}}$: yaleB03

σ	$\frac{\|\widehat{\boldsymbol{L}}-\boldsymbol{L}_0\|_F}{\|\boldsymbol{L}_0\|_F}$	$\frac{\|\widehat{\boldsymbol{S}}-\boldsymbol{S}_0\|_F}{\|\boldsymbol{S}_0\|_F}$	Time (s)	Iter
0	0.0336	0.2128	272.8555	2194
10	0.0458	0.3823	175.4205	1417
20	0.0780	0.5887	261.3707	1519
30	0.1133	0.8008	221.5380	1751
40	0.1469	1.0114	512.7160	4051

Table 10: StablePCP$_u$: yaleB03

σ	$\frac{\|\widehat{\boldsymbol{L}}-\boldsymbol{L}_0\|_F}{\|\boldsymbol{L}_0\|_F}$	$\frac{\|\widehat{\boldsymbol{S}}-\boldsymbol{S}_0\|_F}{\|\boldsymbol{S}_0\|_F}$	Time (s)	Iter
0	0.0336	0.2128	594.5691	5000+
10	0.0434	0.3687	594.4220	5000+
20	0.0760	0.6162	596.9680	5000+
30	0.1109	0.8440	839.4338	5000+
40	0.1449	1.0662	601.5731	5000+

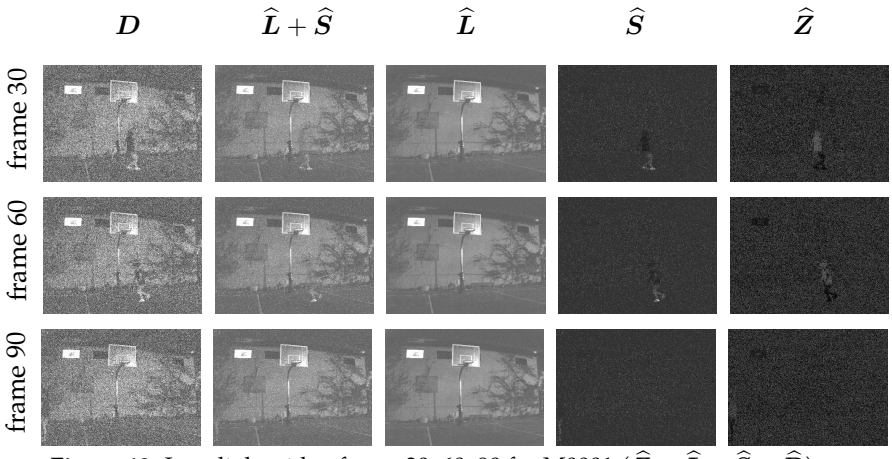


Figure 19: Low light video frame 30, 60, 90 for M0001 ($\widehat{\boldsymbol{Z}} = \widehat{\boldsymbol{L}} + \widehat{\boldsymbol{S}} - \widehat{\boldsymbol{D}}$).

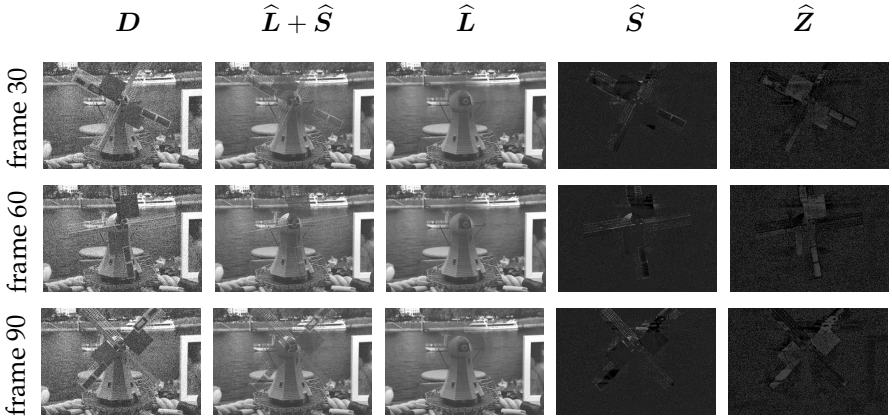


Figure 20: Low light video frame 30, 60, 90 for M0004 ($\widehat{\boldsymbol{Z}} = \widehat{\boldsymbol{L}} + \widehat{\boldsymbol{S}} - \widehat{\boldsymbol{D}}$).

We also provide heatmaps for the relative recovery error, i.e. the 10-average of $\eta_{\text{rel}}(\mu) := \|(\widehat{\boldsymbol{L}}(\mu), \widehat{\boldsymbol{S}}(\mu)) - (\boldsymbol{L}_0, \boldsymbol{S}_0)\|_F / \|(\boldsymbol{L}_0, \boldsymbol{S}_0)\|_F$, in Figure 23.

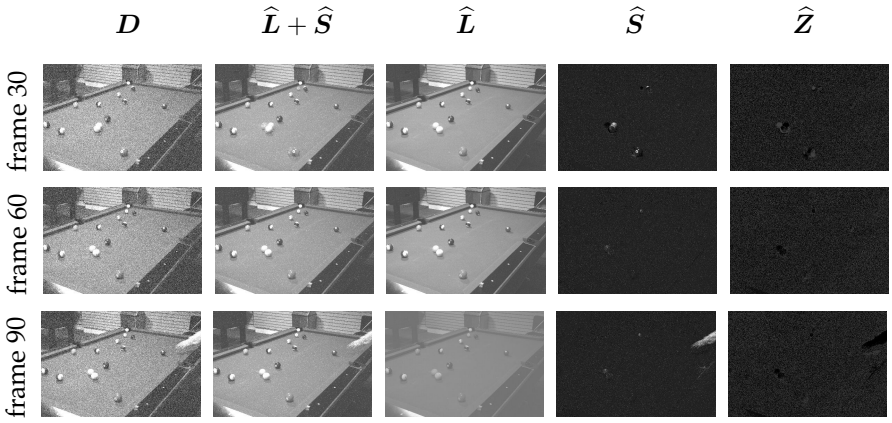
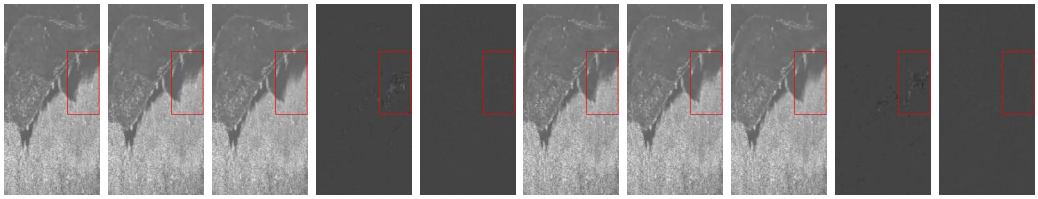


Figure 21: Low light video frame 30, 60, 90 for M0009 ($\widehat{\boldsymbol{Z}} = \widehat{\boldsymbol{L}} + \widehat{\boldsymbol{S}} - \widehat{\boldsymbol{D}}$).

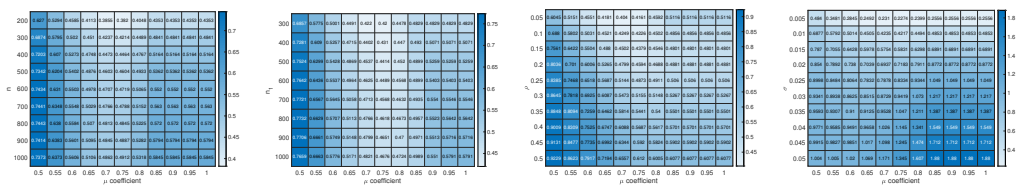


(a) $\boldsymbol{D}$ (b) $\widehat{\boldsymbol{L}}+\widehat{\boldsymbol{S}}$ (c) $\widehat{\boldsymbol{L}}$ (d) $\widehat{\boldsymbol{S}}$ (e) $\widehat{\boldsymbol{Z}}$ (f) $\boldsymbol{D}$ (g) $\widehat{\boldsymbol{L}}+\widehat{\boldsymbol{S}}$ (h) $\widehat{\boldsymbol{L}}$ (i) $\widehat{\boldsymbol{S}}$ (j) $\widehat{\boldsymbol{Z}}$

Figure 22: OCT, a-e): frame 150, f-j): frame 200 ($\widehat{\boldsymbol{Z}} = \widehat{\boldsymbol{L}} + \widehat{\boldsymbol{S}} - \widehat{\boldsymbol{D}}$).

Table 11: Parameters for Simulation: $\rho_S = 0.1$, $|(\boldsymbol{S}_0)_{(i,j)\in\Omega}| = 0.05$

n_1	n_2	ρ_L	σ
$\{200, 300, \ldots, 1000\}$	$n_2 = n_1$	0.1	0.01
$\{300, \ldots, 1000\}$	300	0.1	0.01
300	300	$\{0.05, 0.1, \ldots, 0.5\}$	0.01
300	300	0.1	$\{0.005, 0.01, \ldots, 0.05\}$



(a) vary $n = n_1 = n_2$ (b) vary n_1 (c) vary ρ_L (d) vary σ

Figure 23: $\eta_{\text{rel}}(\mu)$ under different varying parameters